0026-895X/03/6302-311–324$7.00
MOLECULAR PHARMACOLOGY
Vol. 63, No. 2
2110/1036102
*Mol Pharmacol* 63:311–324, 2003
*Printed in U.S.A.*


# Relating Neuronal Nicotinic Acetylcholine Receptor Subtypes Defined by Subunit Composition and Channel Function

QIANG NAI, J. MICHAEL MCINTOSH, and JOSEPH F. MARGIOTTA

*Department of Anatomy and Neurobiology, Medical College of Ohio, Toledo, Ohio (Q.N., J.F.M.); and Department of Biology, University of Utah, Salt Lake City, Utah (J.M.M.)*

Received August 27, 2002; accepted October 21, 2002

This article is available online at http://molpharm.aspetjournals.org

## ABSTRACT

Neuronal nicotinic acetylcholine receptors (nAChRs) are widespread, diverse ion channels involved in synaptic signaling, addiction, and disease. Despite their importance, the relationship between native nAChR subunit composition and function remains poorly defined. Chick ciliary ganglion neurons express two major nAChR types: those recognized by $\alpha$-bungarotoxin ($\alpha$Bgt), nearly all of which contain only $\alpha7$ subunits ($\alpha7$-nAChRs) and those insensitive to $\alpha$Bgt, which contain $\alpha3$, $\alpha5$, $\beta4$, and, in some cases, $\beta2$ subunits ($\alpha3^*$-nAChRs). We explored the relationship between nAChR composition and channel function using toxins recognizing $\alpha7$ subunits ($\alpha$Bgt), and $\alpha3/\beta4$ ($\alpha$-conotoxin-AuIB), or $\alpha3/\beta2$ ($\alpha$-conotoxin-MII) subunit interfaces to perturb responses induced by nicotine, $\alpha7$-, or $\alpha3$-selective agonists (GTS-21 or epibatidine, respectively). Using these reagents, fast-decaying whole-cell current components were attributed solely to $\alpha7$-nAChRs, and slow-decaying components mostly to $\alpha3^*$-nAChRs. In outside-out patches, nicotine activated brief 60- and 80-pS single nAChR channel events, and mixed-duration 25- and 40-pS nAChR events. Subsequently, 60- and 80-pS nAChR events and most brief 25- and 40-pS events were attributed to $\alpha7$-nAChRs, and long 25- and 40-pS events to $\alpha3^*$-nAChRs. $\alpha3^*$-nAChRs lacking $\beta2$ subunits seemed responsible for long 25 pS nAChR events, whereas those containing $\beta2$ subunits mediated the long 40 pS nAChR events that dominate single-channel records. These results reveal greater functional heterogeneity for $\alpha7$-nAChRs than previously expected and indicate that $\beta2$ subunits contribute importantly to $\alpha3^*$-nAChR function. By linking structural to functional nAChR subtypes, the findings also illustrate a useful pharmacological strategy for selectively targeting nAChRs.

Neuronal nAChRs mediate transmission and modulate transmitter release at autonomic and central synapses, are involved in addiction and neurological disease, and participate in key developmental processes (Role and Berg, 1996; Weiland et al., 2000; Dani, 2001; Dani et al., 2001; Rezvani and Levin, 2001; Margiotta and Pugh, 2003). Consistent with their multiple functions, neuronal nAChRs are heterogeneous, assembling as homopentamers of $\alpha7$ or $\alpha8$ subunits or as heteropentamers containing $\alpha2$, $\alpha3$, $\alpha4$, or $\alpha6$ subunits in combination with $\alpha5$, $\beta2$, $\beta3$, and/or $\beta4$ subunits (Sargent, 1993; Margiotta and Pugh, 2003). Examples of native nAChRs defined by subunit composition are relatively rare, however, and the relationship between nAChR composition and function virtually unknown. Such information would be useful for experimental or therapeutic studies requiring subtype-specific intervention.

To relate receptor composition to channel function, we probed nAChRs on ciliary ganglion neurons with subunit-selective agonists and toxin antagonists. Ciliary ganglion neurons are particularly useful for such studies because they express diverse nAChRs that have known subunit composition (Vernallis et al., 1993; Conroy and Berg, 1995) and channel properties (McNerney et al., 2000). One nAChR type is recognized by $\alpha$-bungarotoxin ($\alpha$Bgt), which targets $\alpha7$ subunits with high affinity (Couturier et al., 1990) and labels about $10^6$ surface sites per neuron (McNerney et al., 2000). Approximately 95% of $\alpha$Bgt-nAChRs contain only $\alpha7$ subunits ($\alpha7$-nAChRs); however, 5% lack $\alpha7$ or any known nAChR subunits, and $\alpha$Bgt-nAChRs comprising this minor subtype are termed $\alpha$T35-nAChRs (Vernallis et al., 1993; Pugh et al., 1995). A second nAChR type ($\alpha3^*$-nAChR) is undetected by $\alpha$Bgt but recognized by mAb35, an antibody that detects $\alpha3$ and $\alpha5$ subunits (Conroy and Berg, 1998) and labels about $6 \times 10^4$ surface sites per neuron (Margiotta and Gurantz, 1989). In immunoprecipitation studies, $\alpha3^*$-nAChRs were found to contain $\alpha3$, $\beta4$, and $\alpha5$ subunits, with 20% also containing $\beta2$ subunits (Vernallis et al., 1993; Conroy and Berg, 1995). Functionally, nAChR agonists induce whole-cell currents featuring rapidly and slowly decaying

This work was supported by National Institutes of Health grants DA53316 (to J.F.M.) and MH53631 and GM48677 (to J.M.M.).

**ABBREVIATIONS:** nAChR, nicotinic acetylcholine receptor; $\alpha$Bgt, $\alpha$-bungarotoxin; $\alpha$CTx-AuIB, $\alpha$-conotoxin-AuIB; $\alpha$CTx-MII, $\alpha$-Conotoxin MII; RS, recording solution; Nic, nicotine hydrogen tartrate; Epi, epibatidine dihydrochloride; GTS-21, 3-(2,4-dimethoxybenzylidene)anabaseine; MLA, methyllycaconitine; dTC, *d*-tubocurarine chloride.

components (Zhang et al., 1994), which are loosely associated with the four nAChR subtypes defined above and mediated by four discrete nAChR channel conductance classes (McNerney et al., 2000).

Our approach was to activate whole-cell and single-channel nAChR currents with either a pan-specific agonist (nicotine) or agonists selective for $\alpha$7- (GTS-21) or $\alpha$3-containing (epibatidine) nAChRs (Gerzanich et al., 1995; Meyer et al., 1997; Papke et al., 2000). The contributions of $\alpha$Bgt- and $\alpha$3*-nAChR subtypes were then assessed by comparing the currents with those obtained from neurons treated with $\alpha$Bgt, $\alpha$-conotoxin-AuIB ($\alpha$CTx-AuIB), or $\alpha$-conotoxin-MII ($\alpha$CTx-MII). The latter two are "$\alpha3\beta$-selective", recognizing recombinant $\alpha3\beta4$ and $\alpha3\beta2$ nAChRs, respectively, in *X. laevis* oocytes (Cartier et al., 1996; Luo et al., 1998). The use of subunit selective agonists and toxins combined with whole-cell and single-channel recordings allowed us to relate functional nAChR channels to defined molecular subtypes. Although this strategy relies on available structural information, it avoids uncertainties about subunit assembly and compensatory changes that can make results based on heterologous expression and genetic deletion difficult to interpret (reviewed in Margiotta and Pugh, 2003).

## Materials and Methods

### Neuron and Substrate Preparation

Ciliary ganglion neurons were dissociated from embryonic day 14 (E14) ganglia using collagenase A treatment (0.33 mg/ml 10 min) and mechanical trituration protocols described previously (e.g., Margiotta and Gurantz, 1989; Pardi and Margiotta, 1999; McNerney et al., 2000). Dissociated neurons were suspended in a recording solution (RS) containing 145.0 mM NaCl, 5.3 mM KCl, 0.8 mM $MgSO_4$, 5.4 mM $CaCl_2$, 5.6 mM glucose, and 5.0 mM HEPES acid, pH 7.4, that was supplemented with 10% heat-inactivated horse serum ($RS^{+hs}$). As substrate, glass coverslips (12-mm diameter; Corning, Palo Alto, CA) were acid-washed and 300-kDa poly-(D-lysine) (2 mg/ml in 0.13 M Borate buffer, pH 8.5) applied to each for 12 to 16 h at 4°C. The coverslips were then washed 10 times with distilled water, air-dried, and suspended neurons were plated at 2 to 3 ganglion equivalents per coverslip. Neurons attached to the substrate within 30 min but were allowed to equilibrate for at 37°C for 1 to 3 h before use.

### Electrophysiology

**Whole-Cell Current Acquisition and Analysis.** Neuron recordings were obtained in $RS^{+hs}$ at room temperature (21–24°C) using procedures similar to those described previously (Margiotta and Gurantz, 1989; Pardi and Margiotta, 1999; McNerney et al., 2000). Patch pipettes were pulled from Corning 8161 glass tubing, filled with an intracellular solution containing 145.6 mM CsCl, 1.2 mM $CaCl_2$, 2.0 mM EGTA, 15.4 mM glucose, and 5.0 mM Na-HEPES, pH 7.3, and had tip impedances of 1.5 to 3.0 MΩ when measured in $RS^{+hs}$. Whole-cell currents were collected at −70 mV and filtered at 10 kHz using an Axopatch 200B amplifier (Axon Instruments, Union City, CA). The currents were digitized at 2 kHz using a Tl-125 interface controlled by Clampex (pClamp 6.0; Axon Instruments) and stored on a PC-compatible computer (Gateway, Poway, CA). Membrane capacitance compensation was achieved by eliminating the capacitive current transient in response to a −10 mV pulse using the amplifier series resistance ($R_s$) and capacitance ($C_m$) controls. To activate nAChRs, agonists [i.e., nicotine hydrogen tartrate (Nic), epibatidine dihydrochloride (Epi), or 3-(2,4-dimethoxybenzylidene-)anabaseine (GTS-21)] were dissolved in RS at the desired final concentration from ≥500× frozen stocks and focally applied to individual neuron somata for 2.5 s. The agonists were delivered by pressure microperfusion activated by a computer-driven valve (Picospritzer II; General Valve Co., Waltham, MA) from patch pipettes (Microhematocrit; VWR Scientific Inc., Westchester PA) using two modifications of described previously protocols (Margiotta and Gurantz, 1989; McNerney et al., 2000). First, to ensure efficient agonist exposure, the neurons selected were small, having soma diameters (distributed around a modal value of 11.0 ± 3.1 μm; N >750) that corresponded to those of the choroid neuron population (McNerney et al., 2000). The present findings are also likely to apply to ciliary neurons, however, because both choroid and ciliary neurons express the same subset of nAChR genes (Corriveau and Berg, 1993) and because the properties of individual nAChR channels on the two neuron populations are indistinguishable (McNerney et al., 2000). Second, the perfusion pipette tips were larger (4–6 μm diameter) and delivered higher pressures (8–10 psi) than those used previously. The increased pipette size and pressure resulted in relatively fast agonist delivery that equilibrated in 20 to 30 ms, as estimated from junction current measurements using open tip pipettes. Although slower than the delivery obtained with fast perfusion driven by piezoelectric switching, pressure microperfusion was simpler and proved sufficient to adequately identify the contributions from $\alpha$Bgt- and $\alpha$3*-nAChRs. Apart from some slowing of the fastest component of $\alpha$Bgt-nAChR current decay ($\tau_f$, see below), pressure microperfusion yielded neuronal response parameters (Table 1) that were very similar to those we and others obtained previously using fast piezoelectric switching (Zhang et al., 1994; Pardi and Margiotta, 1999; McNerney et al., 2000). In particular, for neurons of similar small size ($C_m \approx$ 7–12 pF) the peak $\alpha$Bgt-nAChR currents induced by 20 μM Nic applied using piezoelectric switching (−3495 ± 400 pA, $n$ = 12; McNerney et al., 2000) or pressure microperfusion (−3095 ± 240 pA, $n$ = 29; present study) were indistinguishable ($p > 0.1$), indicating that the initial fast component amplitudes are similarly resolved using either method.

Whole-cell currents induced by nAChR agonists were analyzed off-line using Clampfit (pClamp 6.0; Axon Instruments). The time variant current ($I_t$) induced by a saturating agonist dose (e.g., 20 μM Nic) features a sharp transition to peak ($I_{peak}$) representing nAChR activation, followed by rapid and then slower decay phases representing nAChR desensitization (Zhang et al., 1994; Pardi and Margiotta, 1999; McNerney et al., 2000). In such cases, the decay is well described by the sum of three exponential functions given by

$$I_t = A_f \exp(-t/\tau_f) + A_i \exp(-t/\tau_i) + A_s \exp(-t/\tau_s) \quad (1)$$

TABLE 1

Whole-cell response parameters for three nAChR agonists

All values are presented as mean ± S.E.M., and were derived from whole-cell current responses to 20 μM Nic ($n$ = 91), 30 μM GTS-21 ($n$ = 19) or 30 μM Epi ($n$ = 20), all applied for 2.5 s at −70 mV. In each case, specific peak currents (in pA/pF) and time constants ($\tau$) are tabulated for the fast, intermediate, and slow kinetic components, determined as described under *Materials and Methods* and in Fig. 1.

| | Nic | | | GTS-21 | | | Epi | | |
|---|---|---|---|---|---|---|---|---|---|
| Parameter | Fast | Int | Slow | Fast | Int | Slow | Fast | Int | Slow |
| $A/C_m$ (-pA/pF) | 213 ± 12 | 91 ± 7 | 65 ± 3 | 162 ± 23 | 70 ± 7* | 13 ± 2* | 161 ± 40 | 295 ± 37* | 112 ± 8* |
| $\tau$ (ms) | 16 ± 1 | 174 ± 16 | 3360 ± 250 | 19 ± 3 | 84 ± 8* | 690 ± 100* | 28 ± 6* | 170 ± 28 | 1880 ± 200* |

Int, intermediate.

* Significant difference ($p < 0.05$) compared with those obtained with Nic.

In eq. 1, $A_f$, $A_i$, and $A_s$ represent the amplitudes of the fast, intermediate and slow current components at time $t = 0$ from $I_{peak}$, and $\tau_f$, $\tau_i$, and $\tau_s$ indicate the fast, intermediate, and slow decay time constants, respectively such that $I_{peak} = A_f + A_i + A_s$. Responses obtained in the presence of toxins or in response to low doses of agonist typically required fewer components to describe the current decay. To compare agonists and toxin effects, the component amplitudes (e.g., $I_{peak}$, $A_s$) were normalized for neuron size by dividing their values by $C_m$ such that specific membrane currents are expressed in picoamperes/picofarads. To assess toxin effects on whole-cell currents, mean parameter values obtained in recordings from treated and untreated (control) neurons from the same neuron platings were compared. The statistical significance ($p < 0.05$) of comparisons was determined using Student's unpaired, two-tailed $t$ test, conducted for populations with equal or unequal variances, where applicable.

**Single-Channel Current Acquisition and Analysis.** The procedures for single channel data acquisition were similar to those described previously (McNerney et al., 2000). Briefly, outside-out membrane patches were excised from neuron somata in whole-cell mode, and agonists applied by gentle pressure microperfusion (≈2–5 psi) at holding potentials ranging from −80 to −140 mV. Patch currents were digitized at 50 kHz and filtered at a cutoff frequency ($f_1$) of 10 kHz using the Bessel filter included in the Axopatch 200B and then at 9.3 kHz ($f_2$) during data analysis. These settings yielded a final filter frequency ($f_c$) of 6.8 kHz ($f_c^{-2} = f_1^{-2} + f_2^{-2}$) allowing channel openings ≥98 μs (twice the filter rise time, $t_r = 0.3321/f_c$) to be resolved (Colquhoun and Sigworth, 1995). Single nAChR channel events were detected by visual inspection of transitions from the baseline current and manually selected using Fetchan (pClamp 6.0; Axon Instruments). Only those events exceeding set thresholds for amplitude (2× noise) and duration (100 μs) were accepted for analysis.

Single-channel current amplitudes were compiled in 0.2-pA bins, and the distributions fit with Gaussian functions using a Simplex least-squares algorithm that minimizes the difference between actual and fit values (pSTAT; Axon Instruments). It was usually evident by visual inspection that four Gaussian functions were required to best fit the distributions of single nAChR currents induced by nicotine. This was verified in seven patches by comparing $F$ statistic values obtained from fits conducted with four versus five or three functions. In each of these cases, the fits employing four Gaussian functions were significantly improved over those using three ($p < 0.005$) and not significantly different from those employing five functions ($p > 0.1$). Because individual Gaussian functions overlapped somewhat, the range of each current class was determined by calculating the critical amplitudes ($A_c$) between peaks in the distribution that minimized misclassified events from adjacent ranges, as described previously (Colquhoun and Sigworth, 1995). In a few cases, single channel conductances were determined from slopes of the mean current amplitude for each range in the distribution plotted versus the holding potential and were about 25, 40, 60, and 80 pS. In most other cases in which recordings were obtained at a single voltage (−100 mV), channel conductances were estimated for each current class by assuming a reversal potential of −10 mV.

For kinetic analysis, event open durations associated with the four conductance classes were compiled in logarithmic histograms and fitted by maximum likelihood methods using Intrv5 [Interval Analysis 3.12 (1994), generously provided by Dr. Barry S. Pallotta, University of North Carolina, Chapel Hill, NC]. Such histograms revealed heterogeneous open durations requiring up to three time constants (brief, intermediate, and long) to adequately fit the distribution of 25- and 40-pS openings, and up to two time constants (brief and intermediate) for the 60- and 80-pS openings. To assess toxin and agonist effects, the contribution of each channel conductance class ($x$ = 25, 40, 60, or 80 pS) was determined empirically. This was accomplished by calculating the average open probability ($P_{open,x}$) using $\%P_{open,x} = 100\ (\Sigma_{t,x})/TL_x$, where $T$ represents the total record length, $\Sigma_{t,x}$ is the summed open durations of conductance class $x$, and $L_x$ is the number of channels of that class in the patch. $L_x$ was estimated from the number of current levels detected in each recording that corresponded to class $x$, and by visual inspection of the records, was usually 1 or 2. $\%P_{open,x}$ was calculated separately for the very brief and longer open duration kinetic categories apparent for the 25- and 40-pS events using a cutoff value of 200 μs (see *Results*). All single-channel parameters are expressed as mean ± S.E.M,, and the statistical significance ($p < 0.05$) of comparisons was determined using Student's unpaired, two-tailed $t$ test, conducted for populations with equal or unequal variances, where applicable.

**Materials.** Fertilized white Leghorn chicken eggs were obtained from Hertzfeld Poultry Farms (Waterville, OH) and maintained at 37°C in a forced air draft incubator at 100% humidity. αBgt was obtained from Biotoxins, Inc. (St. Cloud, FL), and GTS-21 was generously provided by Dr. W. Kem (University of Florida College of Medicine, Tampa, FL). Most other reagents were purchased from Sigma (St. Louis, MO).

## Results

### Whole-Cell Studies

**Nicotine Activates Both αBgt- and α3*-nAChRs.** Whole-cell responses to Nic were used as a baseline for comparing the actions of subunit-specific toxins and agonists on αBgt- and α3*-nAChR populations. Nic applied at 20 μM induces whole-cell currents that activate within 20 ms ($I_{peak}$) and then decay because of nAChR desensitization as described by eq. 1 (Fig. 1A). Previous findings indicate that the most rapidly decaying component of this response is attributable to αBgt-nAChRs (Zhang et al., 1994; McNerney et al., 2000) because $A_f$ is absent in neurons treated with αBgt (60 nM, 30–60 min; see, e.g., Fig. 1B). αBgt has also been shown to inhibit a somewhat slower decaying component of the Nic response (Zhang et al., 1994) and in the present study it also reduced $A_i$ by 95% (data not shown). Because both $A_f$ and $A_i$ were blocked by αBgt, they have been combined into a single parameter ($I_{fast} = A_f + A_i$) to quantify toxin effects (Fig. 2). Unlike $I_{fast}$, only a minor portion of the slow-decaying component ($A_s$) of the Nic response has been attributed to αBgt-nAChRs (Liu and Berg, 1999). Consistent with these findings, αBgt had a small yet significant effect on $A_s$, corresponding to a 25% reduction in mean slow current density ($A_s/C_m$) compared with untreated controls (Figs. 1B and 2). As depicted in Fig. 1, the decay of $A_s$ was somewhat slower in αBgt-treated neurons; however, comparison of $\tau_s$ for αBgt-treated (3890 ± 386 ms, $n = 60$) and control neurons (Table 1) indicate this trend is not statistically significant ($p > 0.1$). Treating the neurons with the α7-selective antagonist methyllycaconitine (MLA; 50 nM, 1 h) yielded a pattern of inhibition very similar to that of 60 nM αBgt, causing complete block of $A_f/C_m$, a 90% reduction in $A_i/C_m$, and a 30% reduction in $A_s/C_m$ ($n = 11$; data not shown). These findings, obtained with α7-selective antagonists and supported by results presented below using α7- and α3-selective agonists, indicate that $I_{fast}$ is mediated solely by α7-containing αBgt-nAChRs (α7-nAChRs). Because αBgt does not recognize native α3*-nAChRs (Corriveau and Berg, 1993; Vernallis et al., 1993; Conroy and Berg, 1995; Pugh et al., 1995) and both αBgt and MLA failed to completely block $A_s$, the results further suggest that, on average, about 25% of the slow-decaying current can also be attributed to α7-nAChRs (see below).

**α-Conotoxins Selectively Block α3*-nAChRs.** We assessed the contribution of α3*-nAChRs to $A_s$ using *Conus*

spp. toxins expected to target the two $\alpha$3*-nAChR subtypes present on ciliary ganglion neurons (i.e., $\alpha3\beta4\alpha5$ and $\beta2\alpha3\beta4\alpha5$). The first toxin tested was $\alpha$-CTx-AuIB, which blocks recombinant $\alpha3\beta4$ nAChRs expressed in *X. laevis* oocytes ($IC_{50}$ = 750 nM) and is >100-fold less potent on recombinant $\alpha$7-nAChRs and $\alpha3\beta2$-nAChRs, respectively (Luo et al., 1998). With $\alpha$Bgt present to block the contribution from $\alpha$7-nAChRs, $\alpha$CTx-AuIB applied for 30 to 60 min progressively inhibited the response to 20 $\mu$M Nic ($IC_{50}$ = 350 nM), with a 10 $\mu$M dose sufficient to reduce $A_s$ to nearly zero (Figs. 2 and 3, A, B, and D). $\alpha$CTx-AuIB was specific in the sense that the same 10 $\mu$M dose applied *without* $\alpha$Bgt failed to significantly change $I_{fast}$ (Fig. 2), $\tau_f$, or $\tau_i$ (not shown). Under the latter conditions, 10 $\mu$M $\alpha$CTx-AuIB reduced $A_s/C_m$ by about 85% (Fig. 2), an amount consistent with the 75% contribution of $\alpha$3*-nAChRs to $A_s$ determined in the tests conducted with and without $\alpha$Bgt. The second *Conus* spp. toxin tested was $\alpha$CTx-MII, which blocks recombinant rat $\alpha3\beta2$ nAChRs expressed in *X. laevis* oocytes ($IC_{50}$ = 0.5–3.5 nM) and is 2 orders of magnitude less potent on recombinant $\alpha$7- and $\alpha3\beta4$-nAChRs (Cartier et al., 1996; Harvey et al., 1997). Recent studies indicate that $\alpha$CTx-MII also recognizes nAChRs containing $\alpha$6 subunits in mouse brain (Champtiaux et al., 2002). Although abundant in chick retina, $\alpha$6 mRNA is absent from the chick peripheral nervous system, including the ciliary ganglion (Fucile et al., 1998), making it unlikely that $\alpha$6 contributes to nAChRs in this system. Indeed, $\alpha$CTx-MII was previously shown to block slow, $\alpha$Bgt-insensitive synaptic currents in the chick ciliary ganglion (Ullian et al., 1997; Chen et al., 2001), suggesting that it targets $\alpha$3*-nAChRs on the neurons. With $\alpha$Bgt present to block $\alpha$7-nAChRs, $\alpha$CTx-MII applied for 30 to 60 min progressively inhibited the neuronal responses to 20 $\mu$M Nic, and a 300 nM dose reduced $A_s/C_m$ by 90% (Figs. 2 and 3, A, C, and D). Although $\alpha$CTx-MII was more potent for these native neuronal nAChRs ($IC_{50}$ = 33 nM) than $\alpha$CTx-AuIB, it was less potent than reported previously for recombinant $\alpha3\beta2$ nAChRs (Cartier et al., 1996; Harvey et al., 1997). The lower potency of $\alpha$CTx-MII seen here could reflect post-translational effects or the presence of $\alpha$5 and $\beta$4 subunits in $\alpha$3*-nAChRs. As with $\alpha$CTx-AuIB, however, the block of $A_s$ was specific because the same dose had no effect on components attributable to $\alpha$7-nAChRs. When applied without $\alpha$Bgt, 300 nM $\alpha$CTx-MII failed to detectably alter $I_{fast}$ (Fig. 2), $\tau_f$, or $\tau_i$ (data not shown). Once again, under these conditions, $A_s/C_m$

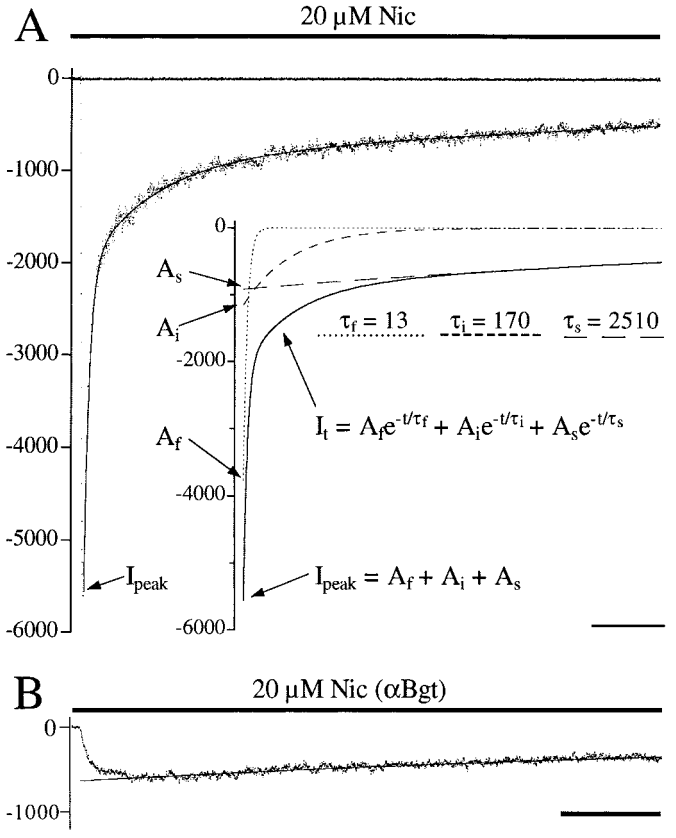


**Fig. 1.** Whole-cell currents induced by nicotine display $\alpha$Bgt-sensitive and -insensitive kinetic components. A, rapid microperfusion with a maximal Nic concentration (20 $\mu$M, horizontal bar) induced a peak whole-cell response ($I_{peak}$) of −5700 pA in this neuron ($C_m$ = 12 pF) corresponding to a specific peak response ($I_{peak}/C_m$) of −475 pA/pF. The holding potential for all whole-cell recordings was −70 mV. Inset. The currents decaying from $I_{peak}$ for the neuron depicted in A are well described by the sum of three exponential functions (eq. 1). The peak amplitudes of the individual fast ($A_f$), intermediate ($A_i$), and slow ($A_s$) current components (arrows at left) corresponded to specific values of −305, −94, and −75 pA/pF, respectively (compare with values in Table 1). The time-dependent contributions of fast, intermediate, and slow components to the current are shown as dotted, short-dashed, and long-dashed lines, respectively, with associated time constants ($\tau_f$, $\tau_i$, and $\tau_s$; in milliseconds) shown for each. The solid line represents the sum of the three components and is also overlaid on the actual current decay in A. B, response to 20 $\mu$M Nic after treating neurons with $\alpha$Bgt (60 nM, 30–60 min). In the neuron depicted ($C_m$ = 11 pF), only the slowly decaying current ($\tau_s$ = 3490 ms) remains, corresponding to a specific response of −60 pA/pF. Calibration bars indicate 250 ms, with that shown in B also applying to the main part of A.

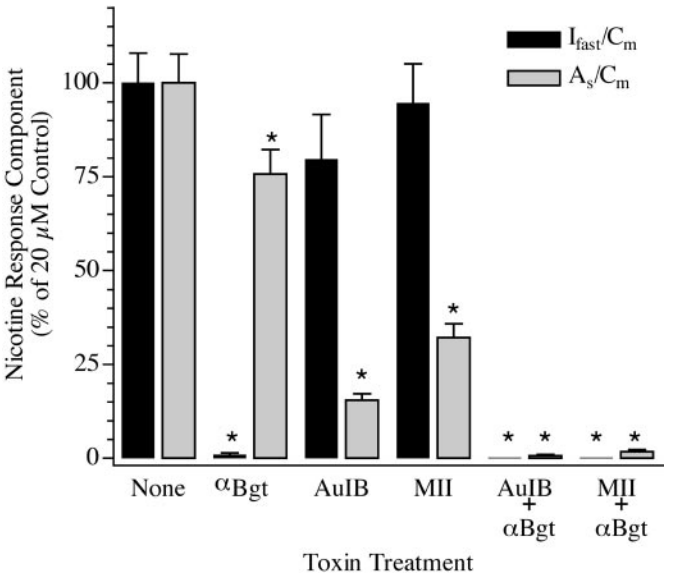


**Fig. 2.** Summary of subunit-specific toxin effects on whole-cell responses to 20 $\mu$M nicotine. $I_{fast}/C_m$ (■) represents the sum of specific fast and intermediate response components [$(A_f + A_i)/C_m$], whereas $A_s/C_m$ (▨) represents the specific slow component alone. Results were compiled from 10 to 60 recordings from toxin-treated neurons and are expressed as the mean (±S.E.M.) percentage of the indicated response component obtained in similar numbers of control neurons from the same experiments. AuIB and MII represent $\alpha$CTx-AuIB and $\alpha$CTx-MII, respectively. Toxins were applied for 30 to 60 min at concentrations that produced maximal block of the response to 20 $\mu$M Nic (60 nM $\alpha$Bgt, 300 nM $\alpha$CTx-MII, 10 $\mu$M $\alpha$CTx-AuIB) and were present in both the bath and the agonist-application pipettes. Bars with asterisks above indicate that the parameter values were significantly different ($p < 0.05$) from those for control neurons; bars without asterisks indicate the values were not detectably different ($p > 0.05$) from control values.

was reduced by about 70%, in accord with a major yet not exclusive contribution of $\alpha$3*-nAChRs to the slowly decaying current. The residual slow currents seen in the presence of $\alpha$CTx-AuIB or $\alpha$CTx-MII decayed with $\tau_s$ of 1100 and 800 ms, respectively, values that were not statistically different from that obtained for slow currents induced by the $\alpha$7-nAChR selective agonist, GTS-21 (see below and Table 1). These results indicate that $\alpha$CTx-AuIB and -MII are potent antagonists for native $\alpha$3*-nAChRs on ciliary ganglion neurons, and support findings obtained with $\alpha$Bgt and MLA suggesting that both $\alpha$3*- and $\alpha$7-nAChRs contribute to slowly decaying whole-cell responses induced by 20 $\mu$M Nic.

**GTS-21 Selectively Activates $\alpha$7-nAChRs.** To further assess the activation of $\alpha$7-nAChRs and their contribution to whole-cell currents, we analyzed responses to GTS-21 (Fig. 4, Table 1), an $\alpha$7-selective agonist also known as DMXB (Kem, 1997; Meyer et al., 1997; Papke et al., 2000). GTS-21 induced inward currents mediated solely by nicotinic nAChRs because they were completely blocked by the classic antagonist *d*-tubocurarine (dTC, 100 $\mu$M, not shown). The currents increased over a range of GTS-21 concentrations (Fig. 4, A and C), with the largest $I_{peak}$ values attained at about 30 $\mu$M ($EC_{50} \approx$ 10–15 $\mu$M). When applied at doses higher than 30 $\mu$M, GTS-21 induced progressively smaller peak responses, consistent with the ability of agonists to block nAChRs when applied at high concentration. The efficacy of 30 $\mu$M GTS-21 in activating $\alpha$7-nAChRs was comparable with that of 20 $\mu$M Nic because values of $A_f/C_m$ were indistinguishable, and those of $A_i/C_m$ were within 25%, for the two agonists (Table

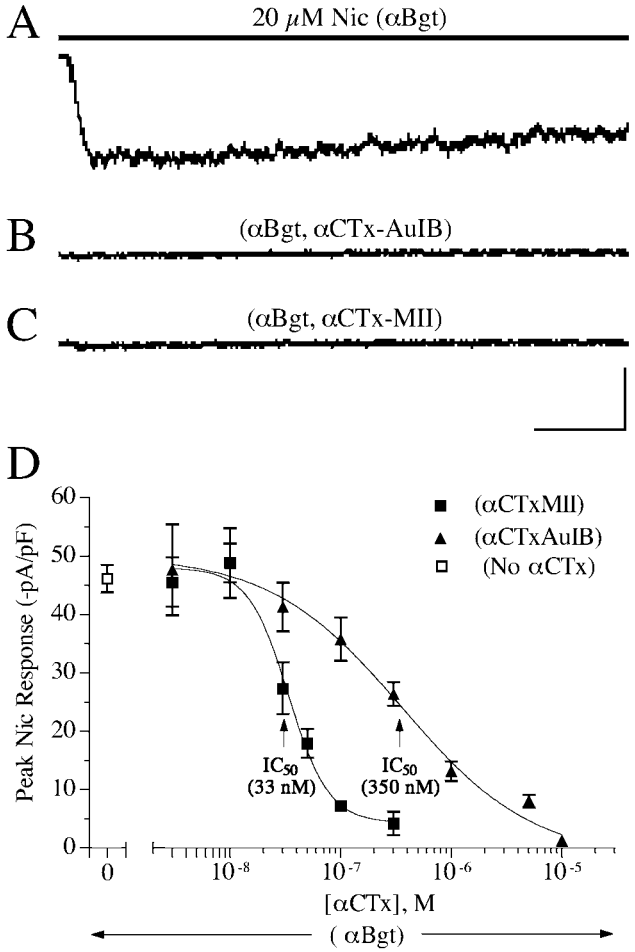


**Fig. 3.** $\alpha$-Conotoxins block $\alpha$3*nAChR-mediated slow-decaying currents. A–C, both $\alpha$CTx-AuIB (B, 10 $\mu$M) and $\alpha$CTx-MII (C, 300 nM) block the slowly decaying current that persists in the presence of 60 nM $\alpha$Bgt (A). Calibration bars indicate 500 pA and 250 ms. D, dose-inhibition relation for $\alpha$-conotoxin effects on the peak residual slow current. Mean $A_s/C_m$ values of (± S.E.M.) are depicted for $\alpha$Bgt-treated neurons (□; $n$ = 60) or for neurons treated with $\alpha$Bgt and the indicated $\alpha$-conotoxin applied at varying concentrations (filled symbols; $n$ = 7–18). $A_s/C_m$ values were fit by nonlinear regression analyses using the Hill equation. Arrowheads indicate the fit-derived concentrations of each $\alpha$-conotoxin predicted to produce half-maximal inhibition ($IC_{50}$) of $A_s/C_m$ (350 and 33 nM for $\alpha$CTx-AuIB and -MII, receptively).

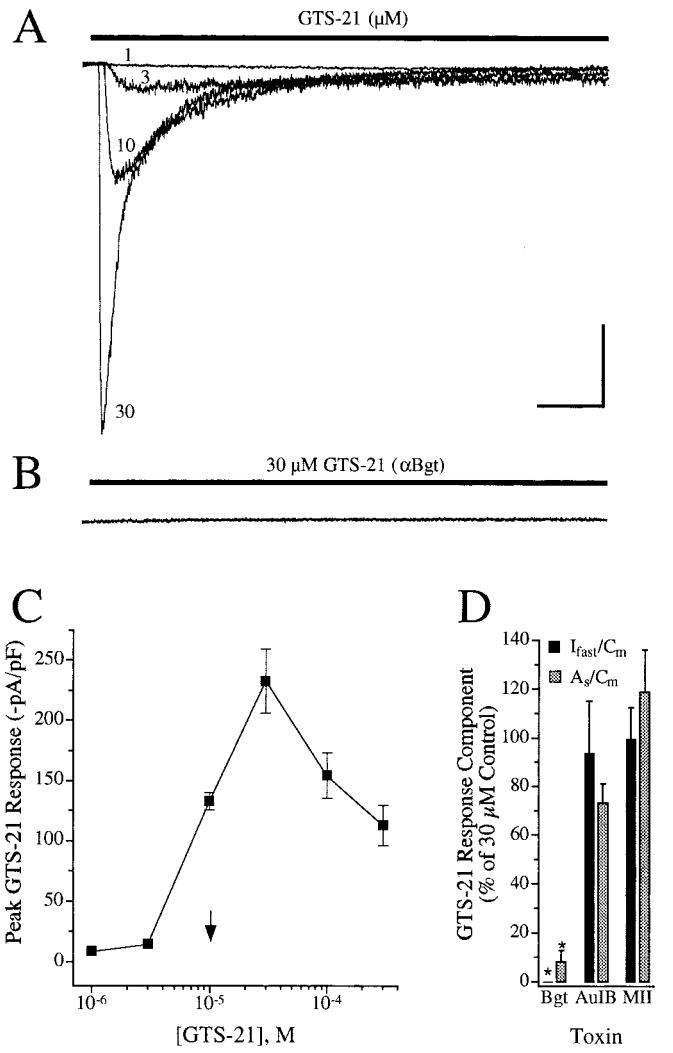


**Fig. 4.** GTS-21 selectively activates $\alpha$Bgt-nAChRs. A, increasing concentrations of GTS-21 (1, 3, 10, and 30 $\mu$M) induce progressively larger peak inward currents. B, the response to 30 $\mu$M GTS-21 is blocked by $\alpha$Bgt. Calibration bars indicate 1 nA and 100 ms. C, dose-response relation for GTS-21. Arrow indicates the approximate GTS-21 concentration required to induce half-maximal $I_{peak}/C_m$ ($EC_{50}$ = 10–15 $\mu$M). Responses were obtained from 8 to 20 neurons at each concentration. Note that GTS-21 concentrations higher than 30 $\mu$M inhibit the response. D, summary of subunit-specific toxin effects on fast- and slow-component whole-cell responses to 30 $\mu$M GTS-21. Toxins were applied and results expressed as described in Fig. 2. Note that $\alpha$Bgt abolished $I_{fast}/C_m$ and inhibited $A_s/C_m$ by >90% ($n$ = 8). The nominal changes in $I_{fast}/C_m$ and $A_s/C_m$ seen after treatments with $\alpha$CTx-AuIB ($n$ = 5) or $\alpha$CTx-MII ($n$ = 7), however, were not statistically significantly ($p > 0.1$ for each). Bars with asterisks above indicate that the parameter values were significantly different ($p < 0.05$) from those for control neurons; bars without asterisks indicate the values were not detectably different ($p > 0.05$) from control values.

1). The kinetics of fast and intermediate current decay displayed a similar pattern, with values of $\tau_f$ identical, and those of $\tau_i$ within a factor of 2, for the two agonists. In accord with the minor contribution of $\alpha$7-nAChRs to slow currents determined using Nic, applications of 30 $\mu$M GTS-21 yielded mean $A_s/C_m$ values that were only 20% of those obtained with 20 $\mu$M Nic. As expected for an $\alpha$7-selective agonist, the fast, intermediate, and slow whole-cell current components induced by 30 $\mu$M GTS-21 were all blocked by 90% or more when neurons were pretreated with $\alpha$Bgt (Fig. 4, B and D). Interestingly, none of the currents induced by GTS-21 application were detectably affected by $\alpha$CTx-AuIB or $\alpha$CTX-MII (Fig. 3D), toxins that recognize and block recombinant $\alpha3\beta4$ and $\alpha3\beta2$ nAChRs, respectively, but have 10- and 400-fold lower potency for recombinant $\alpha$7-nAChRs (Cartier et al., 1996; Luo et al., 1998). Choline has been shown to activate $\alpha$7-nAChRs on rat brain neurons; because it is a partial agonist for $\alpha3\beta4$-containing nAChRs on PC12 cells (Alkondon et al., 1997), we were concerned that it would also activate $\alpha$3*-nAChRs in our system. Indeed, using $\alpha$Bgt or MLA to block the contribution from $\alpha$7-nAChRs, we found that 1 mM choline still evoked substantial whole-cell currents, as well as long 25- and 40-pS single channel currents indicative of $\alpha$3*-nAChR (Nai and Margiotta, unpublished observations; see below). These results indicated that choline would not adequately discriminate between $\alpha$7- and $\alpha$3*-nAChRs on chick ciliary ganglion neurons. By contrast, whole-cell results obtained with GTS-21 as well as single-channel results presented below indicate this agonist is highly selective for $\alpha$7-containing $\alpha$Bgt-nAChRs on the neurons. Given these considerations, the whole-cell findings using Nic and GTS-21 support the idea that $\alpha$7-nAChRs, in addition to underlying fast and intermediate decaying responses, also contribute to a more slowly decaying current. The slow current consistently decayed more rapidly when induced by GTS-21 than Nic (Table 1). Because $\alpha$7-nAChRs underlie nearly all of the slow-decaying current induced by GTS-21 whereas $\alpha$3*-nAChRs underlie most of that induced by Nic, this observation seems likely to reflect inherent differences in slow desensitization kinetics of the two receptor types. Considering the dominant contribution of $\alpha$3*-nAChRs to $A_s$ induced by 20 $\mu$M Nic, such differences are consistent with the nominal increase in $\tau_s$ seen after $\alpha$Bgt-treatment (Fig. 1, Table 1).

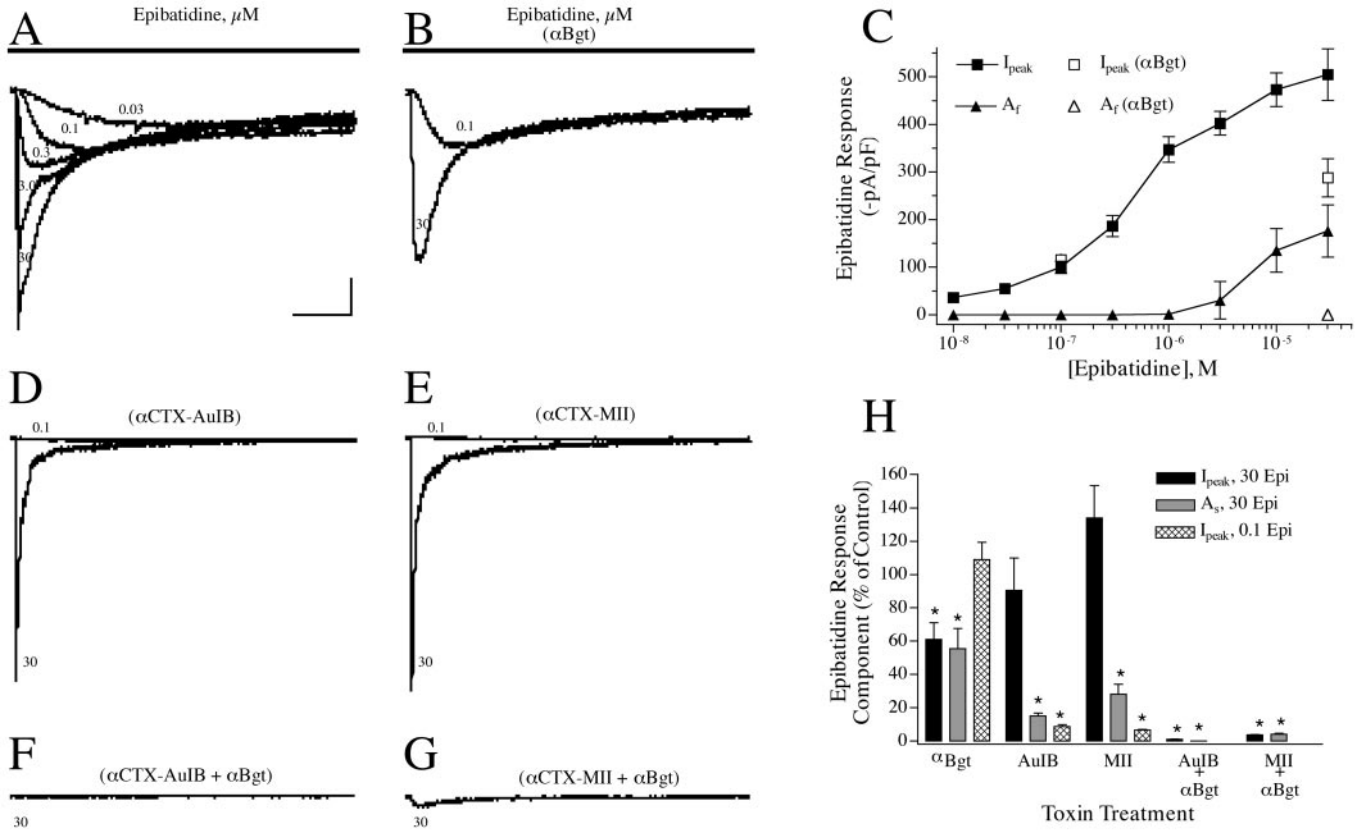


**Fig. 5.** Low doses of epibatidine selectively activate $\alpha$3*-nAChRs. A, Increasing Epi concentrations (0.03, 0.1, 0.3, 3, and 30 $\mu$M) evoke progressively larger whole-cell currents. B, responses to 0.1 $\mu$M EPI decay slowly and are unaffected by $\alpha$Bgt (60 nM), whereas those induced by 30 $\mu$M Epi feature both slow, $\alpha$Bgt-insensitive and fast, $\alpha$Bgt-sensitive decay components (compare with A). C, dose-response relation for Epi. Note that fast decay components (▲) make a negligible contribution to $I_{peak}$ (■) at low Epi concentrations but that this contribution, correlated with $\alpha$Bgt-nAChRs by its sensitivity to $\alpha$Bgt (△, □) increases at concentrations above 1 $\mu$M. Mean $I_{peak}/C_m$ and $A_f/C_m$ (±S.E.M.) values depicted were obtained from 9 to 24 neurons at each Epi concentration. D–E, $\alpha$CTx-AuIB (D) and $\alpha$CTx-MII (E) abolish response to 0.1 $\mu$M Epi and greatly attenuate the slow-decaying response component induced by 30 $\mu$M Epi, indicating that both arise from $\alpha$3*-nAChRs. F–G, the unmasked fast decay response component induced by 30 $\mu$M Epi, is mediated by $\alpha$Bgt-nAChRs because it is blocked when $\alpha$Bgt is coapplied with either $\alpha$-conotoxin. Calibration bars indicate 1 nA and 250 ms. H. Summary of subunit-specific toxin effects on fast and slow component whole-cell responses to 0.1 and 30 $\mu$M Epi ($n$ = 6 to 14 neurons for each condition). Results are expressed as described in Fig. 2. Bars with asterisks above indicate that the parameter values were significantly different ($p < 0.05$) from those for control neurons; bars without asterisks indicate the values were not detectably different ($p > 0.05$) from control values. Note that 0.1 $\mu$M Epi selectively activates $\alpha$Bgt-insensitive, $\alpha$-conotoxin–sensitive $\alpha$3*-nAChRs, whereas at 30 $\mu$M, the agonist also activates $\alpha$Bgt-nAChRs. Toxins were applied in B and D-H as described in Fig. 2.

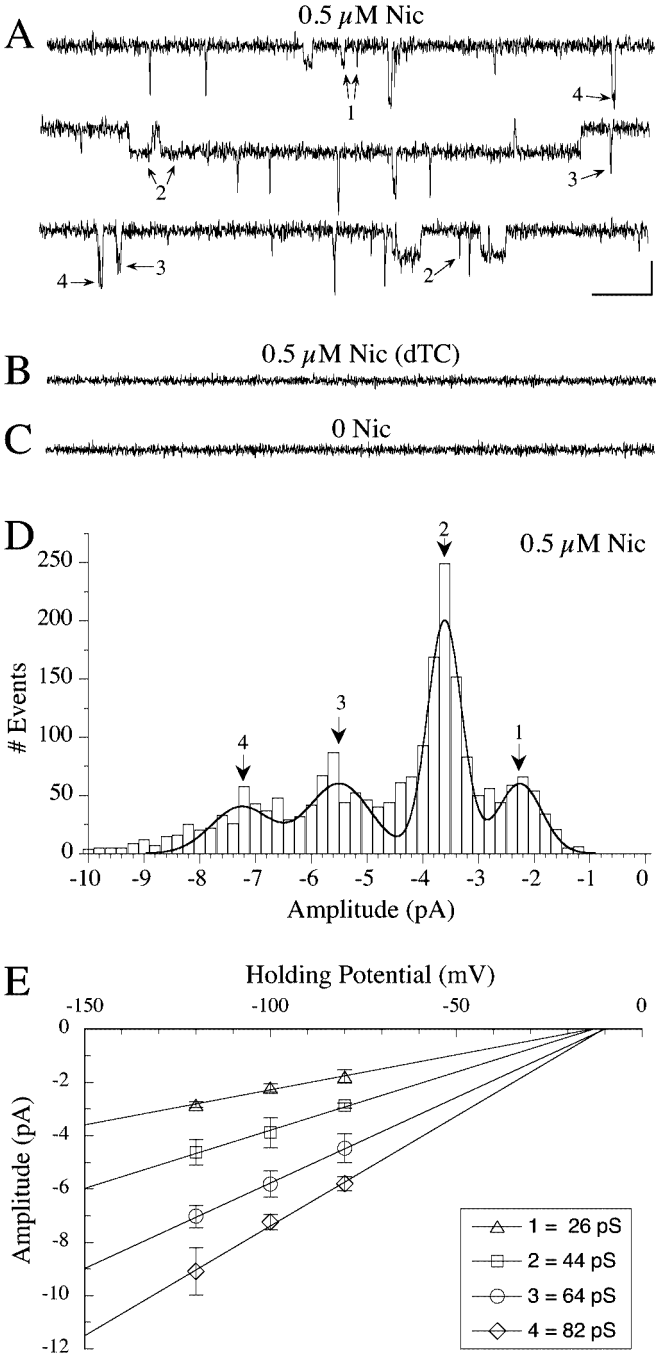


**Fig. 6.** Nicotine activates heterogeneous single-channel currents. A–C, Nic (0.5 $\mu$M) applied to an outside-out patch activated single-channel events at four (1, 2, 3, 4) discrete current levels (A). The currents arise from nAChRs because they were abolished by dTC (B, 100 $\mu$M) and absent when the patch perfusate lacked agonist (C). Calibration bars indicate 5 pA and 5 ms. Patches were held at $-100$ mV, and the currents sampled at 20-$\mu$s intervals and filtered at $f_c$ = 6.8 kHz, allowing detection of open or closed durations $\geq$100 $\mu$s (see *Materials and Methods*). D, single-channel amplitude histogram with four modal peaks reflecting mean current amplitudes corresponding to the four current levels in A. Note that current events of about $-3.5$ pA (level 2) predominate. E, current-voltage plots reveal four distinct nAChR channel slope conductances (indicated in box) for the patch depicted in A. The currents at each level reversed at about $-10$ mV. Overall, the conductances associated with channel current classes 1, 2, 3, and 4 were about 25, 40, 60, and 80 pS (means, 26, 42, 61, and 83 pS; $n$ = 26), respectively.

**Epibatidine Selectively Activates $\alpha$3*-nAChRs.** Using heterologously expressed nAChRs in *X. laevis* oocytes, epibatidine (Epi) was previously shown to be 100-fold more potent for chicken $\alpha3\beta4$ and $\alpha3\beta2$ nAChRs than for $\alpha$7-nAChR homomers (Gerzanich et al., 1995). We therefore examined the ability of Epi to preferentially activate native $\alpha$3*-nAChRs on ciliary ganglion neurons. Epi induced graded whole-cell currents (Fig. 5A) that were mediated solely by nicotinic nAChRs because they were completely blocked by dTC (not shown). Peak Epi-induced currents increased over a range of concentrations, with the maximal responses attained at about 30 $\mu$M ($EC_{50}$ = 0.56 $\mu$M; Fig. 5, A and C). As with Nic and GTS-21, a fast Epi response component ($A_f$) was apparent but only at relatively high concentrations (3–30 $\mu$M). We attribute this fast component to activation of $\alpha$7-nAChRs having relatively low affinity for Epi for two reasons. First, $\alpha$Bgt blocked $A_f$ and reduced $I_{peak}$ by a complementary amount in neurons challenged with 30 $\mu$M Epi, whereas the toxin had no detectable effect on $I_{peak}$ in neurons challenged with 0.1 $\mu$M Epi (Fig. 5, B and C). Second, the Epi dose-response relation predicts a 15-fold lower apparent affinity for the $\alpha$Bgt-sensitive $A_f$ ($EC_{50}$ = 6 $\mu$M) than for the toxin-insensitive portion of the peak response ($I_{peak} - A_f$) ($EC_{50}$ = 0.4 $\mu$M). At concentrations $\leq$1 $\mu$M, however, Epi seemed selective for $\alpha$3*-nAChRs. In particular, responses obtained using 0.1 $\mu$M Epi were insensitive to $\alpha$Bgt (Fig. 5, B and H) and blocked by $\alpha$CTx (Fig. 5, D, E, and H). These findings are in good agreement with results from expression studies (Gerzanich et al., 1995), and indicate that when applied at low concentration, Epi will preferentially activate $\alpha$3*- over $\alpha$7-nAChRs on ciliary ganglion neurons.

**Combining $\alpha$3*-nAChR Selective Agonists and Antagonists.** The specificity of the two *Conus* spp. toxins for $\alpha$3*- over $\alpha$Bgt-nAChRs demonstrated using Nic was tested further using agonists selective for the two nAChR types. We expected that the $\alpha3\beta$-selective conotoxins would be ineffective in blocking currents induced by the $\alpha$7-nAChR selective agonist GTS-21 but highly potent in blocking currents induced by the $\alpha$3*-nAChR selective agonist Epi, and both expectations were borne out. After treating ciliary ganglion neurons with $\alpha$CTx-AuIB or $\alpha$CTx-MII at doses sufficient to block the $\alpha$3*-nAChR attributable responses to 20 $\mu$M Nic (10 $\mu$M and 300 nM, respectively) the fast, intermediate, and slow components of whole-cell currents induced by 30 $\mu$M GTS21 were unchanged (Fig. 4D). Conversely, the same conotoxin treatments reduced $I_{peak}$ in response to 0.1 $\mu$M Epi by $>$90%, and reduced $A_s$ in response to 30 $\mu$M Epi by about 80% (Fig. 5, D, E, and H). In the presence of either *Conus* spp. toxin (Fig. 5, D and E), 30 $\mu$M Epi induced a large, rapidly-decaying peak current that was indistinguishable from $I_{peak}$ in control neurons. We attribute this rapidly decaying peak current to $\alpha$7-nAChRs, usually masked by the somewhat slower-decaying $\alpha$Bgt-insensitive component seen in control neurons. When applied in conjunction with $\alpha$Bgt to block the contribution from $\alpha$7-nAChRs, $\alpha$CTx-MII further attenuated, and $\alpha$CTx-AuIB abolished, peak responses to 30 $\mu$M Epi (Fig. 5, F, G, and H). These findings indicate that $\alpha$Bgt and both conotoxins are useful as specific antagonists for whole-cell currents mediated by $\alpha$Bgt- and $\alpha$3*-nAChRs, respectively, on ciliary ganglion neurons. The ability of $\alpha$CTx-MII, a presumed $\alpha3\beta2$ selective toxin, to block 90% of the $\alpha$3*-nAChR mediated slow current seemed at odds with the previous

demonstration that only about 20% of surface $\alpha$3*-nAChRs contain $\beta$2 and hence a potential $\alpha3\beta2$ interface. An explanation for this finding may be that, because of differences in channel properties, $\alpha$3*-nAChRs containing $\beta$2 make a greater contribution to whole-cell currents than those lacking $\beta$2. This issue is addressed below.

### Single-Channel Studies

**Nicotine Activates 25-, 40-, 60-, and 80-pS nAChRs That Have Distinct Kinetic Properties.** Single-channel studies were performed to correlate effects of the nAChR-specific agonists and toxins, as determined in whole-cell studies, with functional channel types. In outside-out neuron patches held at −100 mV, perfusion with 0.5 $\mu$M Nic activated single nAChR channel currents in four distinct amplitude ranges (1–4 in Fig. 6, A and D). The currents reflected nAChR activation because none were observed when the perfusion buffer lacked agonist or when the bath and perfusion buffer contained dTC (Fig. 6, B and C). The four current classes corresponded to nAChR channel conductances of about 25, 40, 60, and 80 pS, with 40-pS events predominating (Fig. 6, D and E). These values are nearly identical to those obtained previously using ACh except that the lowest conductance class scored closer to 30 pS (Margiotta and Gurantz, 1989; McNerney et al., 2000). To investigate nAChR kinetics, open durations corresponding to each conductance class were analyzed in patches in which the total number of events ($N_t$) exceeded 1000 (Fig. 7, Table 2). In these cases, open duration distributions for both 25- and 40-pS classes were well characterized by three mean open time constants [brief ($\tau_b \leq 200$ $\mu$s), intermediate ($200 < \tau_i \leq 1000$ $\mu$s), and long ($\tau_l > 1000$ $\mu$s)] of approximately 50, 500, and 3000 $\mu$s, respectively (Fig. 7, A and B; Table 2). The vast majority of events described by $\tau_b$ (i.e., brief) were <200 $\mu$s in duration, and these comprised about 70 and 50% of the 25- and 40-pS events, respectively. By contrast, >90% of the 60-pS events and >99% the 80-pS

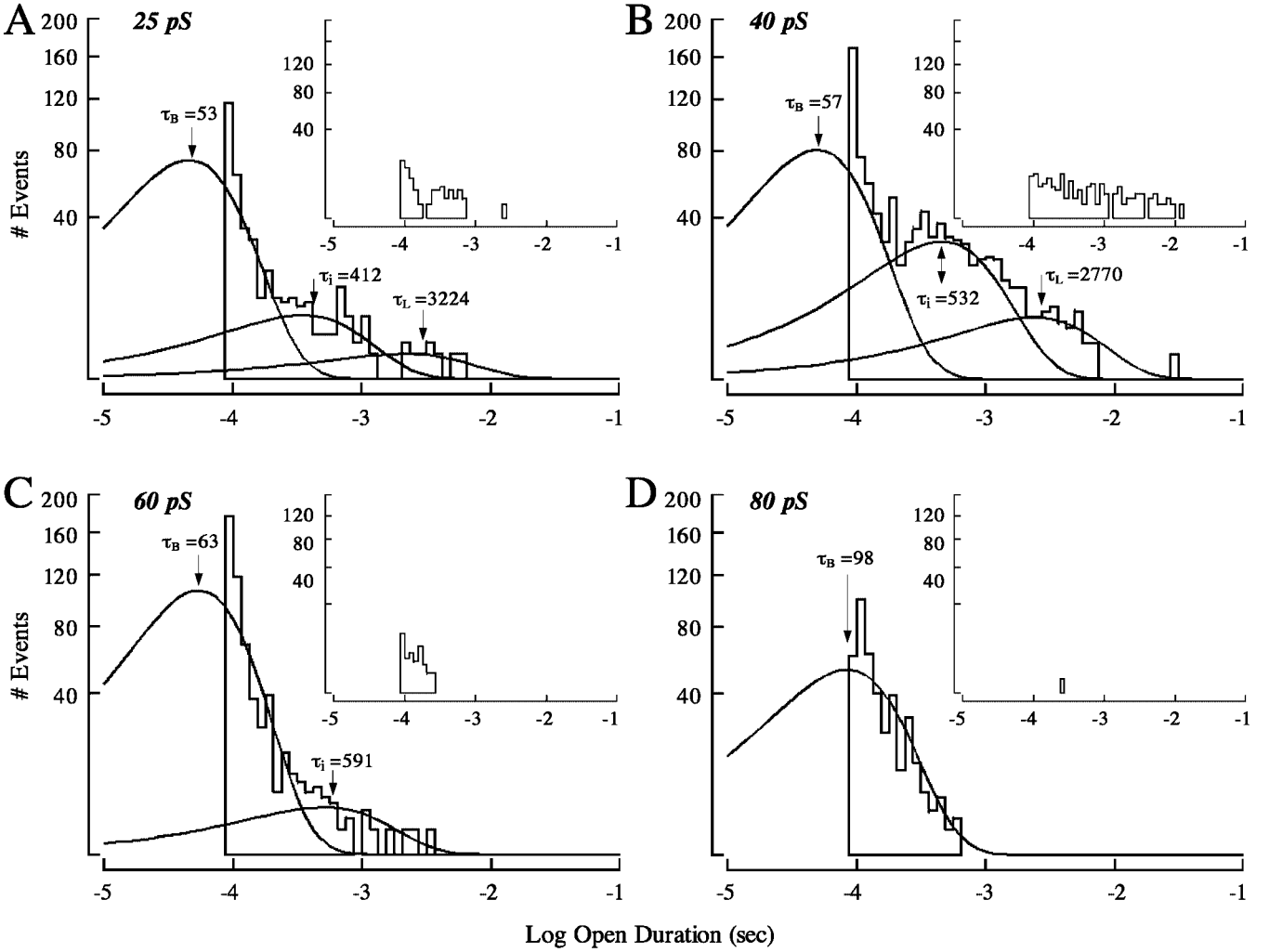


**Fig. 7.** Analysis of open durations for 25- (A), 40- (B), 60- (C), and 80-pS (D) nAChR channels. nAChRs were activated by applying 0.5 $\mu$M Nic to outside-out patches held at −100 mV as in Fig. 6. Nic-induced single channel currents were segregated by amplitudes (see *Materials and Methods*) corresponding to the indicated conductance classes and, in each case, open durations displayed on log duration versus square root axes. Solid lines represent the contributions of brief, intermediate-, and long events, as defined from maximum likelihood fits generated using IntrV (see *Materials and Methods*). Labeled arrows at individual peaks indicate the derived time constants (in microseconds). Note that brief nAChR openings made a major contribution to the histogram area for events in the 25-, 60-, and 80-pS conductance classes ($A_B$ = 69, 89, and 100%, respectively) but not in the 40-pS class ($A_B$ = 35%). The insets show the distribution of open durations for the same event classes obtained after treatment with 60 nM $\alpha$Bgt. Note that $\alpha$Bgt blocked nearly all brief events in every conductance class, without markedly affecting intermediate and long 25- and 40-pS events. Data used in main panels were obtained from the patch depicted in Fig. 6.

TABLE 2
Single-channel parameters for three nAChR agonists

All values are presented as mean ± S.E.M. and were obtained from single channel current records obtained at −100 mV using 0.5 μM Nic, 1 μM GTS-21, or 10 nM Epi, each applied for 40 s. Open time constants ($\tau$) and relative histogram areas (A) for brief (B), intermediate (i) and long (L) openings in each conductance class ($\gamma$) were derived from patches in which the total number of accepted events ($N_T$) exceeded 1000 for Nic ($N_T$ = 1843 ± 287, $n$ = 5 patches), 200 for GTS-21 ($N_T$ = 800 ± 264, $n$ = 4), and 800 for Epi ($N_T$ = 1264 ± 291, $n$ = 7) as outlined in the text. Because events <98 μs were unresolved, $\tau_B$ values should be considered estimates. For all agonists, events with durations ≤200 μs were classified as brief, and those with durations >200 μs were classified as intermediate or long. The cutoff for long events was 1 ms for Nic and GTS-21 and 2 ms for Epi. $P_{open}$ values shown were determined empirically from all patches with $N_T$ > 200 for Nic and Epi ($N_T$ = 749 ± 126, $N_T$ = 26 and 707 ± 142, $n$ = 27, respectively) and $N_T$ > 100 for GTS-21 ($N_T$ = 464 ± 276, $n$ = 8) as described under *Materials and Methods*. $P_{open,brief}$ values were compiled from events with durations ≤200 μs, whereas $P_{open,long}$ values were compiled from events with durations >200 μs (i.e., intermediate and long events). In the patches subjected to detailed kinetic analysis, $P_{open}$ values obtained using the relevant $\tau$ values were indistinguishable from those obtained empirically except for the long 25-pS nAChR events induced by nicotine. In one case, $P_{open,long}$ derived using $\tau_L$ (0.124) was about 2-fold larger than the empirically obtained value.

| | Nic | | | | GTS-21 | | | Epi | | | |
|---|---|---|---|---|---|---|---|---|---|---|---|
| $\gamma$ (pS) | 26.3±0.2 | 42.0±0.3 | 61.1±0.4 | 82.6±0.5 | 25.5±0.6 | 42.9±1.0 | 62.5±0.6 | 82.3±1.0 | 26.1±0.3 | 40.6±0.2 | 60.1±0.5 | 80.3±1.0 |
| $\tau_B$ (μs) | 57±5 | 53±3 | 71±7 | 122±12 | 95±36 | 55±10 | 71±11 | 134±14 | 63±9 | 194*±14 | 60±9 | 115±49 |
| $A_B$ (%) | 70.9±8.5 | 51.9±13.8 | 93.4±2.6 | 99.5±0.6 | 91.5±5.9 | 88.2±6.7* | 88.5±6.5 | 97.6±2.8 | 45.5±12.9 | 29.8±13.2 | 88.6±8.6 | 100 |
| $P_{open,brief}$ (%) | 0.022±0.004 | 0.024±0.004 | 0.068±0.014 | 0.059±0.010 | 0.010±0.003* | 0.025±0.009 | 0.052±0.018 | 0.043±0.016 | 0.009±0.001* | 0.015±0.002* | 0.007±0.002* | 0.003±0.001* |
| $\tau_i$ (μs) | 400±59 | 523±123 | 738±208 | 698 | 632±334 | 370±106 | 624±212 | 545 | 966±203* | 1189±176* | 859±432 | N.D. |
| $A_i$ (%) | 23.3±9.3 | 29.2±10.3 | 2.5±2.2 | 0.5±0.6 | 8.5±5.9 | 10.9±5.8 | 11.5±6.5 | 2.4±2.8 | 38.3±8.6 | 56.0±10.6 | 11.4±8.6 | 0.0±0.0 |
| $\tau_L$ (μs) | 3544±815 | 2790±658 | 2059±540 | N.D. | N.D. | 5659 | N.D. | N.D. | 3689±450 | 4025±607 | N.D. | N.D. |
| $A_L$ (%) | 5.8±3.1 | 18.9±6.0 | 4.0±2.9 | 0.0±0.0 | 0.0±0.0 | 0.9±1.0* | 0.0±0.0 | 0.0±0.0 | 16.1±7.8 | 14.3±7.1 | 0.0±0.0 | 0.0±0.0 |
| $P_{open,long}$ (%) | 0.052±0.010 | 0.399±0.098 | | | 0.011±0.004* | 0.015±0.006* | | | 0.121±0.032* | 0.862±0.154* | | |

N.D., not determined.
* Significant difference ($p$ < 0.05) compared with those obtained with Nic.

events were classified as brief, with the open duration distributions dominated by a single component with $\tau_b$ of about 70 and 120 μs, respectively (Fig. 7, C and D; Table 2).

**αBgt Blocks Brief-Duration 25-, 40-, 60-, and 80-pS nAChR Openings.** To determine which single nAChR currents represent activation of α7-nAChRs, we first assessed the effects of 60 nM αBgt, a dose that blocked $I_{fast}$ by >95% in whole-cell experiments (Fig. 2). When patches excised from neurons treated with the toxin were challenged with 0.5 μM Nic, single channel currents corresponding to the all-brief 60- and 80-pS openings were virtually absent, whereas those corresponding to longer duration 25- and 40-pS openings were preserved (Fig. 8A). Inspection of the records and open duration distributions from toxin-treated patches with $N_t$ > 200 further revealed that αBgt also markedly reduced the sizable fraction of brief 25- and 40-pS nAChR openings (Fig. 7, insets). Thus, αBgt seems to target brief, Nic-induced nAChR openings in all four conductance classes. Because the αBgt sensitivity of 25- and 40-pS nAChR events was correlated with open duration, toxin effects were quantified by considering the brief (≤200 μs) 25-, 40-, 60-, and 80-pS events and the longer (>200 μs) 25- and 40-pS events separately. The relative open-time contribution of each conductance and kinetic class to the total record time ($P_{open}$) could then be determined empirically for all patches and the specificity of toxin effects assessed from changes in $P_{open}$ (Fig. 8D). As indicated by analyses of open duration distributions (Fig. 7) brief openings make significant contributions to the total record time. In fact, the combined $P_{open}$ values for brief Nic-induced 25-, 40-, 60-, and 80-pS openings is about 40% of that for the long 25- and 40-pS events (Fig. 8D, Table 2). Consistent with results obtained by comparing distributions of nAChR open durations, $P_{open}$ values obtained with and without αBgt indicate that the toxin selectively targets brief Nic-induced nAChR openings (Fig. 8D). Specifically, αBgt reduced $P_{open}$ values by >95% for the 60- and 80-pS nAChR events, and by >70% for brief 25- and 40-pS events, but failed to significantly change $P_{open}$ for long 25- and 40-pS events ($p$ = 0.08 and 0.18, respectively). In an earlier study, αBgt blocked 60- and 80-pS events but failed to detectably alter $P_{open}$ associated with 25- and 40-pS nAChR openings (McNerney et al., 2000). This is not inconsistent with the present findings because events were previously sorted by conductance alone such that those scoring in 25- and 40-pS classes included long as well as brief openings. Because long 25- and 40-pS openings dominate open times for events in both of these conductance classes (Table 2) and are αBgt-insensitive, the associated $P_{open}$ values for each will seem unchanged when sorted by conductance alone. Patches excised from six cells treated with MLA (50 nM, 1 h) and then challenged with 0.5 μM Nic yielded results that were indistinguishable from those obtained with αBgt (data not shown). In these cases, MLA reduced $P_{open}$ values by >95% for the 60- and 80-pS nAChR events, and by 70% and 60% for brief 25- and 40-pS events, respectively, but failed to detectably change $P_{open}$ for long 25- and 40-pS events ($p$ = 0.84 and 0.08, respectively). Thus results obtained here using two α7-selective antagonists indicate that α7-nAChRs underlie both the majority of brief 25- and 40-pS nAChR events and essentially all 60- and 80-pS events activated by nicotine.

**α-Conotoxins Target Long-Duration 25- and 40-pS nAChR Openings.** Based on their selectivities in whole-cell

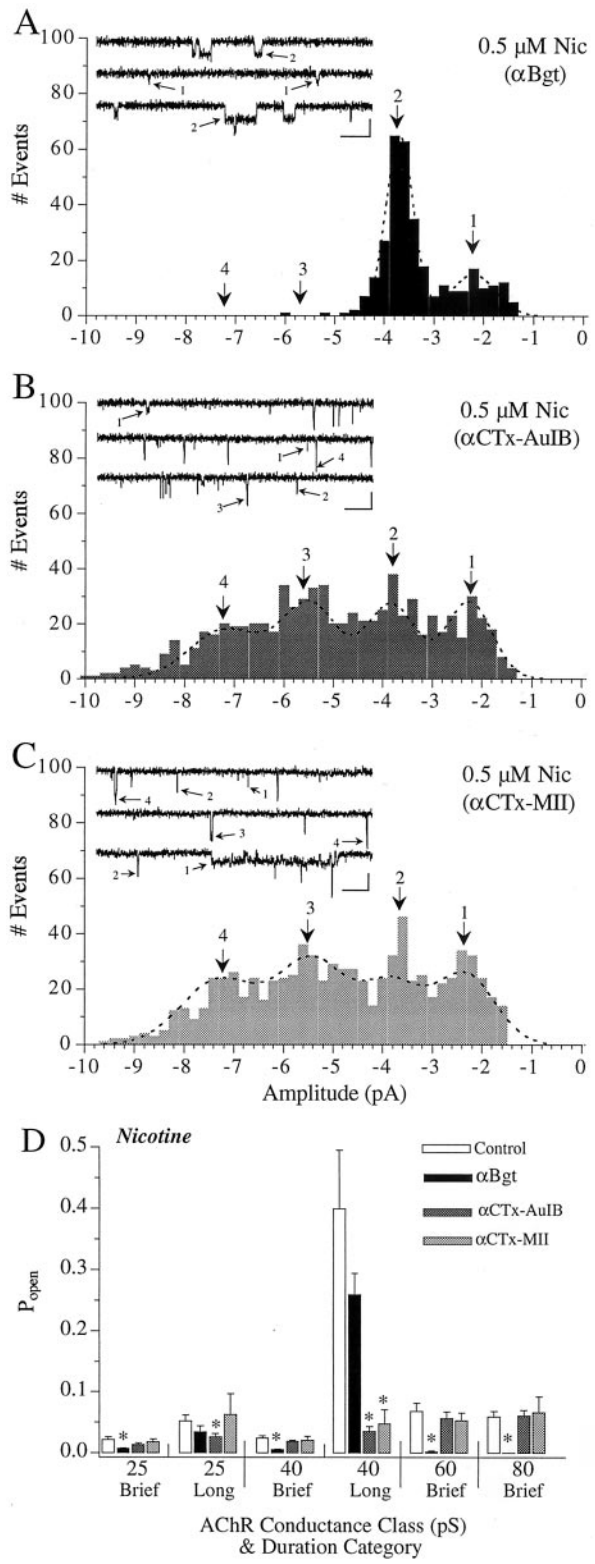


**Fig. 8.** Subunit-selective toxins target different nAChR channel events. A-C, patches were excised from neurons treated with αBgt (A), αCTx-AuIB (B), or αCTx-MII (C) and challenged with 0.5 μM Nic plus the indicated toxin. For each toxin treatment, histograms portray the distribution of event amplitudes acquired in individual 40-s recordings, with sample events depicted in the insets (calibration bars indicate 5 pA and 5 ms). Patches were held at −100 mV, and the currents sampled at 20-μs intervals and filtered at $f_c$ = 6.8 kHz, allowing detection of open or closed durations ≥100 μs (see *Materials and Methods*). As in Fig. 6, the numbers 1, 2, 3, and 4 refer to current events corresponding to nAChR channel conductances of 25, 40, 60, and 80 pS. D, toxin blockade of Nic-induced nAChR openings. nAChR channel events were segregated according to conductance and mean open duration (brief or long), and toxin effects assessed by determining $P_{open}$ associated with the corresponding events for each treatment condition as described in the text. Note that αBgt reduced $P_{open}$ for brief open duration events of all four conductances whereas αCTx-AuIB and αCTx-MII block long 25- and/or 40-pS events, respectively. Apparent reductions in $P_{open}$ for brief 25-pS events after αCTx-AuIB and αCTx-MII treatments, and for long 25-pS after αBgt treatments, were not statistically significant ($p > 0.1$ for each). Results depicted represent mean (±S.E.M.) determinations of $P_{open}$ obtained from 12 to 26 outside-out patch recordings. Toxins were applied as described in Fig. 2.

studies, we next compared the effects of *Conus* spp. toxins with those of αBgt as a means of distinguishing single channel events mediated by α3*- versus α7-nAChRs. Neurons were treated with αCTx-AuIB or αCTx-MII using doses that maximally inhibited Nic-induced whole-cell α3*-nAChR currents (10 μM and 300 nM, respectively) and patches from treated neurons challenged with 0.5 μM Nic plus *Conus* spp. toxin. αCTx-AuIB, which targets the α3/β4 nAChR subunit interface (Luo et al., 1998), inhibited long 25- and 40-pS nAChR events (Fig. 8B), significantly reducing $P_{open}$ associated with each by 50 and 91%, respectively (Fig. 8D). As in whole-cell studies, αCTx-AuIB was specific for α3*-nAChRs in the sense that it failed to detectably change $P_{open}$ for the brief 25-, 40-, 60-, or 80-pS nAChR events associated with α7-nAChRs. Because $P_{open}$ for long 40-pS nAChR events far exceeds that of long 25-pS events, the effect of αCTx-AuIB are in good agreement with its nearly complete block of α3*-nAChRs seen in whole-cell studies. Because about 20% of α3*-nAChRs on ciliary ganglion neurons contain β2, we next tested αCTx-MII, a toxin that targets α3/β2 nAChR interfaces (Cartier et al., 1996). Interestingly, αCTx-MII was specific for long 40-pS nAChR events, inhibiting their appearance, and therefore reducing their $P_{open}$ by 90%, without detectably affecting $P_{open}$ for long 25-pS events ($p = 0.75$) (Fig. 8, C and D). As with αCTx-AuIB, brief 25-, 40-, 60-, and 80-pS events associated with α7-nAChRs were unaffected by αCTx-MII. The inability of either αCTx-AuIB or -MII to affect $P_{open}$ for the brief 25-, 40-, 60-, and 80-pS events further supports the attribution of these events to α7-nAChRs. In addition, the ability of αCTx-AuIB to reduce $P_{open}$ for long 25- and 40-pS nAChR currents is consistent with these events arising from α3*-nAChRs. From the known α3*-nAChR subtypes on the neurons (Vernallis et al., 1993; Conroy and Berg, 1995), and the subunit interface selectivity of αCTx-MII and αCTx-AuIB (Cartier et al., 1996; Luo et al., 1998), the specificity of αCTx-MII observed here further suggests that the long 40- and 25-pS nAChR events are attributable to α3*-nAChR subtypes that contain and lack β2 subunits, respectively. The finding that αCTx-MII selectively blocks long 40-pS events (Fig. 8D) also explains results from whole-cell studies indicating that nearly all of $A_s$ is blocked by the toxin (Figs. 2 and 3) because $P_{open}$ for long 40-pS events greatly exceeds that for long 25-pS events (see Table 2 and *Discussion*).

**GTS-21 and Epibatidine Activate α7- and α3*-nAChR Channels, Respectively.** Single channel results obtained thus far using Nic, a pan-specific agonist for nAChRs, suggest that brief and long nAChR events are attributable to α7- and α3*-nAChR classes, respectively. To further test this hypothesis, we used GTS-21 to preferentially activate α7-

nAChR channels (Fig. 9). As with Nic, perfusion with 1 $\mu$M GTS-21 activated four ranges of single nAChR channel currents corresponding to conductances of about 25, 40, 60 and 80 pS (Fig. 9A, Table 2). GTS-21 efficiently activated brief events in all four conductance classes, displaying $\tau_b$ and $P_{open}$ values that, in nearly all cases, were indistinguishable from those obtained with Nic (Fig. 9B, Table 2). In contrast, GTS-21 failed to effectively induce long 25- and 40-pS nAChR events. Consistent with this relatively low efficacy is the absence of a prominent 40 pS peak in amplitude histograms obtained using GTS-21 (e.g., Fig. 9A), the absence of long events in the open duration distribution (Fig. 9B), and $P_{open}$ values associated with the few long 25- and 40-pS events observed that were 5- and 25-fold lower than those obtained using Nic (Table 2). As seen with Nic, the $P_{open}$ values associated with brief 25-, 40-, 60- and 80-pS nAChR events activated by GTS-21 were specifically and drastically reduced after treatment with $\alpha$Bgt (compare Figs. 8D and 9C). $\alpha$Bgt reduced $P_{open}$ by 70% for brief 25 pS events and by >95% for brief 40-, 60-, and 80-pS events. In addition, $P_{open}$ values for the few long 25- and 40-pS events normally induced by GTS-21 were unaffected by treatment with $\alpha$Bgt ($p = 0.48$ and 0.85, respectively). Because GTS-21 is an $\alpha$7-selective agonist (Meyer et al., 1997; Papke et al., 2000), these results further support the idea that the majority of brief 25- and 40-pS nAChR openings and virtually all 60- and 80-pS nAChR openings arise from $\alpha$7-nAChRs.

We next performed a series of complementary experiments using epibatidine (Epi), applied at a low concentration to selectively activate $\alpha$3*- over $\alpha$7-nAChR channels (Fig. 5). Epi (10 nM) primarily activated long 25- and 40-pS nAChR openings (Fig. 10, A and B) and was more effective in this regard than was Nic, as seen by 2-fold larger $\tau_i$ and $P_{open}$ values obtained with Epi for both event classes (Table 2). In contrast, Epi activated brief events very poorly compared with Nic, as seen by significantly lower values of $P_{open}$ associated with all brief events, particularly the all-brief 60- and 80-pS events, with these displaying 10- and 20-fold lower $P_{open}$ values for Epi compared with Nic. Consistent with the specificity of Epi for $\alpha$3*-nAChRs seen in whole-cell studies, treatment with $\alpha$CTx-AuIB or -MII failed to change $P_{open}$ values associated with brief 25-, 40-, 60-, and 80-pS events. In addition, the *Conus* spp. toxin effects on long 25- and 40-pS events induced by Epi mirrored those obtained with Nic (compare Figs. 8D and 10C). Specifically, $\alpha$CTx-AuIB treatment lowered $P_{open}$ for both the Epi-induced 25- and 40-pS long events by 71 and 92%, respectively. In addition, $\alpha$CTx-MII reduced $P_{open}$ for 40-pS long events by 97% and, as seen with Nic, $\alpha$CTx-MII failed to significantly affect $P_{open}$ for 25 pS long events ($p = 0.08$). These results, obtained with an $\alpha$3-selective agonist, are consistent with those obtained using Nic, further indicating that long 25- and 40-pS events represent activation of $\alpha$3*-nAChRs. Given the composition of $\alpha$3*-nAChRs, and the specificities of $\alpha$CTx-AuIB and -MII the findings also strongly suggest that 25- and 40-pS long events can be attributed to $\alpha$3*-nAChRs that lack and contain $\beta$2, respectively.

## Discussion

Two principal conclusions emerge from these studies. One is that $\alpha$Bgt-nAChRs, 95% of which are assembled from $\alpha$7-

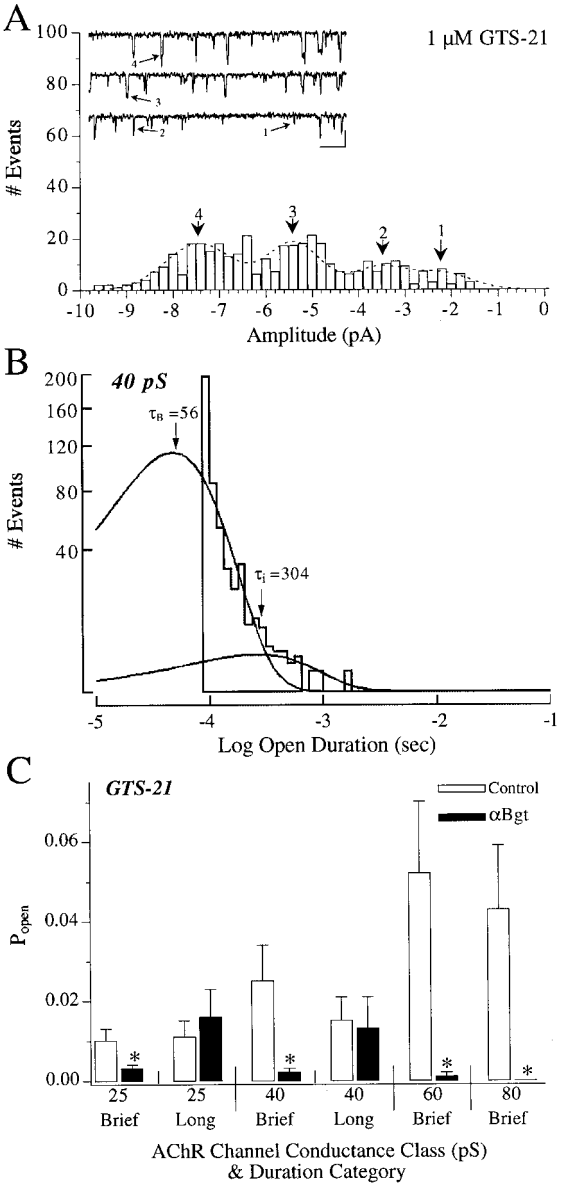


**Fig. 9.** GTS-21 activates brief nAChR openings. A, GTS-21 (1 $\mu$M) applied to an outside-out patch induced all-brief nAChR channel openings at four current levels (1, 2, 3, 4) yielding conductances comparable with those activated by 0.5 $\mu$M Nic (compare with Fig. 6; see Table 2). Calibration, 5 pA and 5 ms. Patches were held at −100 mV, and the currents sampled at 20-$\mu$s intervals and filtered at $f_c = 6.8$ kHz, allowing detection of open or closed durations ≥100 $\mu$s (see *Materials and Methods*). B, analysis of 40-pS nAChR channel openings induced by GTS-21, and conducted as described in Fig. 7. Solid lines represent the contributions of brief and intermediate-duration events, as defined using maximum likelihood fits generated by IntrV (see *Materials and Methods*). Labeled arrows at individual peaks indicate the derived time constants (in microseconds). Note the reduction in intermediate-duration and virtual absence of long 40 pS nAChR openings (compare with Fig. 7B). C, summary of $\alpha$Bgt effects on GTS-21 induced nAChR openings. Channel openings were categorized and toxin effects were assessed as described in Fig. 8. Note that $\alpha$Bgt reduced $P_{open}$ for brief nAChR events in all four conductance classes activated by GTS-21 but did not effect the few long 25- and 40-pS openings induced by this agonist. Results depicted represent mean (±S.E.M.) determinations of $P_{open}$ obtained from 6 toxin-treated and 14 control outside-out patches challenged with 1 $\mu$M GTS-21. $\alpha$Bgt was applied as described in Fig. 2. Bars with asterisks above indicate that the parameter values were significantly different ($p < 0.05$) from those for control neurons; bars without asterisks indicate the values were not detectably different ($p > 0.05$) from control values.

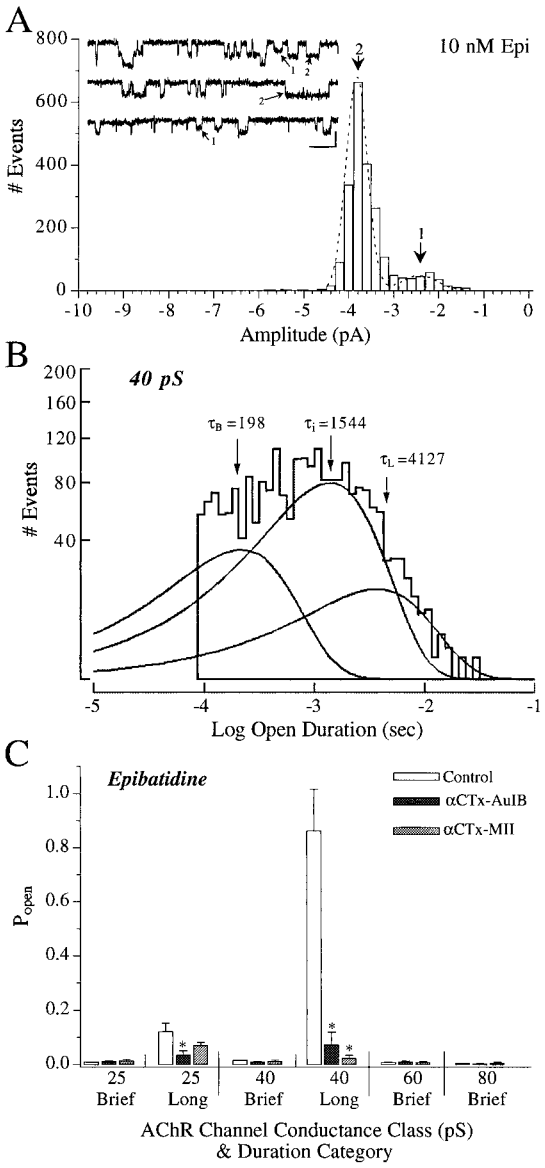


**Fig. 10.** Epibatidine selectively activates long 25- and 40-pS nAChR openings. A, Epi (10 nM) applied to an outside-out patch induced long nAChR channel openings at two current levels (1, 2) yielding conductances of about 25 and 40 pS that were indistinguishable from those activated by 0.5 $\mu$M Nic (compare with Fig. 6; see Table 2). Calibration, 5 pA and 5 ms. Patches were held at −100 mV, and the currents sampled at 20-$\mu$s intervals and filtered at $f_c$ = 6.8 kHz, allowing detection of open or closed durations ≥100 $\mu$s (see *Materials and Methods*). B, analysis of 40-pS nAChR channel openings induced by Epi conducted as described in Fig. 7. Solid lines represent the contributions of intermediate- and long events (see *Materials and Methods*). Labeled arrows at individual peaks indicate the derived time constants (in microseconds). Note the reduction in brief 40 pS nAChR openings and the increase in long events (compare with Fig. 7B). C, summary of $\alpha$-conotoxin effects on Epi-induced nAChR openings. Channel openings were categorized and toxin effects assessed as described in Fig. 8. Note the $\alpha$-conotoxins failed to detectably change $P_{open}$ associated with the few brief 25-, 40-, 60- and 80-pS events activated by Epi. Note also that $\alpha$CTx-AuIB reduced $P_{open}$ values for long 25- and 40-pS nAChR events, whereas $\alpha$CTx-MII reduced $P_{open}$ for long 40-pS nAChR events but not for long 25-pS nAChR events ($p$ = 0.08). Results depicted represent mean (±S.E.M.) determinations of $P_{open}$ obtained from 6 $\alpha$CTx-AuIB treated, 12 $\alpha$CTx-MII treated, and 27 control outside-out patches challenged with 10 nM Epi. $\alpha$-Conotoxins were applied as described in Fig. 2. Bars with asterisks above indicate that the parameter values were significantly different ($p < 0.05$) from those for control neurons; bars without asterisks indicate the values were not detectably different ($p > 0.05$) from control values.

subunits alone (Vernallis et al., 1993; Conroy and Berg, 1995; Pugh et al., 1995) nevertheless underlie diverse nAChR currents. The second is that $\alpha$3*-nAChRs, all of which contain $\alpha$3, $\beta$4, and $\alpha$5 subunits, are functionally enhanced in the subpopulation of these receptors that also contains $\beta$2 subunits. These conclusions are consistent with the specificities of agonists and antagonists used, suggesting that a similar pharmacological strategy can be employed to selectively target nAChR subtypes in other systems.

$\alpha$Bgt-nAChR currents were surprisingly heterogeneous. In addition to fast- and intermediate-decay components, attributable to $\alpha$Bgt-nAChRs by their sensitivity to aBgt (Zhang et al., 1994; Pardi and Margiotta, 1999) and MLA (this study), we found that both Nic and the $\alpha$7-selective agonist GTS-21 generated a slow-decay component blocked by $\alpha$Bgt. These results confirm that $\alpha$7-nAChRs (the major $\alpha$Bgt-nAChR subtype) mediate fast- and intermediate-decay response components but indicate that they also contribute to a more sustained current. The complex decay of $\alpha$7-nAChR whole-cell currents is likely to reflect entry into and recovery from desensitization. Multiple desensitized states have recently been proposed for $\alpha$7-nAChRs in a model that assumes a single fast entry rate but predicts slower, mixed recovery rates depending on the level of agonist occupancy (Papke et al., 2000). Such a model could account for the heterogeneity in whole-cell current decay seen here. Further study is required, however, to determine whether the intermediate and/or slow-decay components of $\alpha$7-nAChR currents reflect slower phases of entry into desensitized states, the appearance of receptors recovering from desensitization at mixed rates, or both.

Nicotine activated single-channel events separable by open duration and conductance. We showed previously that $\alpha$Bgt-nAChRs underlie 60- and 80-pS channel events but were unable to determine whether both represented activation of the $\alpha$7-nAChR subtype (McNerney et al., 2000). We can now attribute the 60- and 80-pS events as well as the brief 25- and 40-pS events to $\alpha$7-nAChRs (Table 3) for several reasons: first, GTS-21 efficiently activated brief nAChR events in each conductance class, whereas the $\alpha$3-selective agonist Epi failed to do so. Second, $\alpha$7-selective antagonists $\alpha$Bgt and MLA blocked the all-brief 60- and 80-pS events induced by Nic, and $\alpha$Bgt blocked these events when induced by GTS-21. Third, $\alpha$Bgt drastically reduced $P_{open}$ for brief 25- and 40-pS events induced by Nic or GTS-21, and MLA similarly inhibited the events when induced by Nic. Fourth, $\alpha3\beta$-selective

TABLE 3

Relating functional and structural nAChR subtypes

Single nAChR channel properties obtained using 0.5 $\mu$M Nic as agonist at left ($\gamma$, $\tau_{open}$, and $P_{open}$) are related to structural subtypes at right. Brief and long indicate $\tau_{open}$ values ≤200 and >200 $\mu$s, respectively. Numerals preceding asterisks represent relative $P_{open}$ values for the indicated channel category. See *Discussion* for details.

| nAChR Function | | | nAChR Structure | |
|---|---|---|---|---|
| $\gamma$ | $\tau_{open}$ | $P_{open}$ | Type | Subtype |
| *pS* | | | | |
| 25 | Brief | 1* | αBgt-nAChR | $(\alpha7)_5$ |
| 40 | Brief | 1* | αBgt-nAChR | $(\alpha7)_5$ |
| 60 | Brief | 2* | αBgt-nAChR | $(\alpha7)_5$ |
| 80 | Brief | 2* | αBgt-nAChR | $(\alpha7)_5$ |
| 25 | Long | 1* | α3*-nAChR | (α3β4α5) |
| 40 | Long | 15* | α3*-nAChR | (β2α3β4α5) |

α-conotoxins failed to detectably change $P_{open}$ for brief events in any conductance class. Fifth, no evidence was obtained for functional correlates of the minor, αT35-αBgt-nAChR subtype previously reported to lack α7- or any of the other known subunits present in the ganglion (Pugh et al., 1995). Overall, the results indicate that, despite their presumed uniform arrangement as α7-homopentamers, α7-nAChRs can adopt multiple conductance states. In fact, unitary single-channel currents induced from α7-nAChRs expressed in cell lines (Ragozzino et al., 1997) in *X. laevis* oocytes (Palma et al., 1997) or in lipid bilayers (Gotti et al., 1997) all display heterogeneous amplitudes that are indicative of at least two conducting states. Multiple conductance states are also observed for cyclic nucleotide-gated channels, where results support a general allosteric model such that openings to each state can occur with agonist bound to fewer than all subunits (Ruiz and Karpen, 1999). Such a model may apply for native α7-nAChRs; however, without further experiments, a concerted model (Monod et al., 1965), with each conducting state directly related to numbers of agonist molecules bound, cannot be excluded. Differential post-translational modification may explain how α7-nAChR homopentamers can display heterogeneity in binding or opening. For example, α7 subunits can exist in two different disulfide-bonded conformations that confer distinct functional properties on assembled α7-nAChRs (Rakhilin et al., 1999). Further studies are needed to determine the relevance of post-translational modifications in regulating the conductance of native α7-nAChRs.

α3*-nAChRs present on ciliary ganglion neurons were functionally identified using α-conotoxins. The presumption that αCTx-AuIB and -MII would target native α3*-nAChR subtypes stems from heterologous expression experiments in which the toxins recognized rodent nAChRs assembled from α3β4 and α3β2 subunits, respectively, but displayed much lower potency for heteromeric neuronal and muscle nAChRs lacking these subunit combinations (Cartier et al., 1996; Luo et al., 1998). Previous studies also suggested the two toxins can recognize appropriate native nAChRs (Ullian et al., 1997; Penn et al., 1998; Quik et al., 1999; Chen et al., 2001). In our whole-cell experiments, both α-conotoxins discriminated broadly between chicken α3*- and αBgt-nAChRs, each producing dose-dependent inhibition of slow-decaying currents induced either by Nic or the α3-selective agonist Epi without affecting fast-decaying currents attributable to αBgt-nAChRs. The whole-cell assays did not allow us to distinguish between the two α3*-nAChR subtypes (α3β4α5 and β2α3β4α5), however, because α-CTx-MII was able to block nearly all of the response attributable to α3*-nAChRs.

The inability of α-CTx-MII to discriminate between α3*-nAChR subtypes in whole-cell assays would arise if the toxin were poorly selective for chicken β2 over β4 when combined with α3, or if individual β2-containing receptors mediate the bulk of α3*-AChR–mediated membrane currents. The first possibility seems unlikely based on analysis of a previous structure-activity study where the major determinants conferring αCTx-MII sensitivity of rodent nAChRs were found to be within amino acids 121 to 195 and 54 to 80 of the α3 and β2 sequences, respectively (Harvey et al., 1997). A BLAST comparison reveals that these motifs are 97% (α3) and 100% (β2) identical between rat and chick subunits. Moreover, the amino acids differing between rat and chick α3 subunits (S164T and E187D), both represent conservative substitutions. These considerations, plus the fact that a nonconservative substitution in rat α3 subunit (E187S) had little effect on αCTx-MII sensitivity (Harvey et al., 1997), indicate the toxin should recognize chicken nAChRs containing α3 and β2 subunits. Although determinants conferring specificity of αCTx-AuIB are unknown, extracellular domains of α3 and β4 are likely involved. In this regard, we restate the 97% homology between the rat and chick α3 extracellular motifs described above and note from additional BLAST comparisons that β4 subunits from rat and chick are 91% homologous over the entire N-terminal extracellular domain. In addition, chimeric rat β subunits constructed using the first 103 residues of β4, with the remainder from β2 (β4-103-β2), displayed little or no sensitivity to αCTx-MII when coexpressed in *X. laevis* oocytes with α3 (Harvey et al., 1997). The simplest conclusion from this analysis is that αCTx-MII recognizes α3/β2 over α3/β4 subunit interfaces in chick nAChRs and does so preferentially over αCTx-AuIB, which recognizes the α3β4 subunit combination found in both α3*-nAChR subtypes.

Single-channel records acquired in the presence of αCTx-AuIB or -MII provided the necessary resolution to identify long 25- and 40-pS events with corresponding α3*-nAChR subtypes (Table 3). As expected for α3*-nAChRs, which all contain α3 and β4 but lack α7, both 25- and 40-pS long events induced by Nic (or Epi) were significantly inhibited by αCTx-AuIB but unaffected by αBgt or MLA. The long 25- and 40-pS events were differentially sensitive, however, to the α3/β2-selective αCTx-MII, which drastically reduced $P_{open}$ associated with long 40 pS events induced by Nic or Epi but failed to detectably alter $P_{open}$ for long 25 pS events. Given the arguments for αCTx-MII specificity presented above, these findings indicate that long 25 pS nAChR events arise from the major α3*-nAChR subtype (α3β4α5), whereas long 40 pS events arise from the minor α3*-nAChR subtype that in addition contains β2 (Table 3). Consistent with the first interpretation, expression of rat α3β4α5 subunits in *X. laevis* oocytes resulted in long single nAChR channel events having a conductance of 24.9 pS (Sivilotti et al., 1997). Although our results indicate that long 40 pS events can be attributed to the numerically minor α3*-nAChR subtype, calculations based on $P_{open}$ and γ values (Table 2, Nic or Epi) indicate they make a far greater contribution to the α3*-nAChR mediated membrane current (92%) than do long 25-pS events (8%). This observation is consistent with the second possibility cited above, and predicts that αCTx-MII, although it selectively targets the minor β2-containing subtype, will nevertheless block nearly all of the α3*-nAChR membrane currents, as was observed. Because long 40-pS events dominated our single channel records we further infer that the presence of β2 subunits strongly enhances the activity of α3*-nAChRs. The enhanced channel function is likely to be associated with changes in the opening and/or closing kinetics as well as conductance. At present, however, the mechanisms responsible for such changes are unknown.

These experiments revealed inherent functional flexibility in α7-nAChRs and the importance of β2 subunits in enhancing α3*-nAChR function. Both conclusions depended on knowledge of nAChR subunits expressed in the ciliary ganglion and on subunit-selective toxins, but neither would have been made if the toxin effects were assessed with whole-cell recording alone. Specifically, although toxin block followed

by whole-cell recording readily predicted broad distinctions between major nAChR types, such recordings were insufficient to reveal functional heterogeneity within $\alpha$7-nAChRs or to distinguish between functional $\alpha$3*-nAChR subtypes. Thus our findings also illustrate the importance of conducting single-channel recordings in parallel with pharmacological manipulations to identify nAChR subtypes with their corresponding functional channels.

**Acknowledgments**

We thank Drs. Darwin Berg, Marthe J. Howard, and Phyllis C. Pugh for helpful discussions on the work and manuscript.

**References**

Alkondon M, Pereira EFR, Cortes WS, Maelicke A, and Albuquerque EX (1997) Choline is a selective agonist of $\alpha$7 nicotinic acetylcholine receptors in the rat brain neurons. *Eur J Neurosci* **9:**2734–2742.

Cartier GE, Yoshikami D, Gray W, Luo S, Olivera B, and McIntosh J (1996) A new $\alpha$-conotoxin which targets $\alpha3\beta2$ nicotinic acetylcholine receptors. *J Biochem* **271:** 7522–7528.

Champtiaux N, Han Z-Y, Bessis A, Rossi FM, Zoli M, Marubio L, McIntosh JM, and Changeux J-P (2002) Distribution and pharmacology of $\alpha$6-containing nicotinic acetylcholine receptors analyzed with mutant mice. *J Neurosci* **22:**1208–1207.

Chen M, Pugh P, and Margiotta J (2001) Nicotinic synapses formed between chick ciliary ganglion neurons in culture resemble those present on the neurons *in vivo.* *J Neurobiol* **47:**265–279.

Colquhoun D and Sigworth FJ (1995) Fitting and statistical analysis of single-channel records, in *Single Channel Recording* (Sakmann B, Neher E eds), pp 483–585, New York: Plenum Press.

Conroy WG and Berg DK (1995) Neurons can maintain multiple classes of nicotinic acetylcholine receptors distinguished by different subunit compositions. *J Biol Chem* **270:**4424–4431.

Conroy WG and Berg DK (1998) Nicotinic receptor subtypes in the developing chick brain: appearance of a species containing the $\alpha$4, $\beta$2 and $\alpha$5 gene products. *Mol Pharmacol* **53:**392–401.

Corriveau RA and Berg DK (1993) Coexpression of multiple acetylcholine receptor genes in neurons: quantification of transcripts during development. *J Neurosci* **13:**2662–2671.

Couturier S, Bertrand D, Matter J-M, Hernandez M-C, Bertrand S, Millar N, Valera S, Barkas T, and Ballivet M (1990) A neuronal nicotinic acetylcholine receptor subunit ($\alpha$7) is developmentally regulated and forms a homo-oligomeric channel blocked by $\alpha$-Btx. *Neuron* **5:**847–496.

Dani JA (2001) Nicotine mechanisms in Alzheimer's disease. Overview of nicotinic receptors and their roles in the central nervous system. *Biol Psychiatry* **49:**166–174.

Dani JA, Ji D, and Zhou FM (2001) Synaptic plasticity and nicotine addiction. *Neuron* **31:**349–352.

Fucile S, Matter J-M, Erkman L, Ragozzino D, Barbaino B, Grassi F, Alemà S, Ballivet M, and Eusebi F (1998) The neuronal $\alpha_6$ subunit forms functional heteromeric acetylcholine receptors in human transfected cells. *Eur J Neurosci* **10:**172–178.

Gerzanich V, Peng X, Wang F, Wells G, Anand R, Fletcher S, and Lindstrom J (1995) Comparative pharmacology of epibatidine: a potent agonist for neuronal nicotinic acetylcholine receptors. *Mol Pharmacol* **48:**774–782.

Gotti C, Moretti M, Maggi R, Longhi R, Hanke W, Klinke N, and Clementi F (1997) Alpha7 and alpha8 nicotinic receptor subtypes immunopurified from chick retina have different immunological, pharmacological and functional properties. *Eur J Neurosci* **9:**1201–1211.

Harvey SC, McIntosh JM, Cartier GE, Maddox FN, and Luetje CW (1997) Determinants of specificity for $\alpha$-contotoxin MII on $\alpha3\beta2$ neuronal nicotinic receptors. *Mol Pharmacol* **51:**336–342.

Kem WR (1997) Alzheimer's drug design based upon an invertebrate toxin (anabaseine) which is a potent nicotinic receptor agonist. *Invert Neurosci* **3:**251–259.

Liu QS and Berg DK (1999) Actin filaments and the opposing actions of CaM Kinase II and calcineurin in regulating alpha7-containing nicotinic receptors on chick ciliary ganglion neurons. *J Neurosci* **19:**10280–10288.

Luo S, Kulak J, Cartier G, Jacobsen R, Yoshikami D, Olivera B, and McIntosh J (1998) $\alpha$-Conotoxin AuIB selectively blocks $\alpha3\beta4$ nicotinic acetylcholine receptors and nicotine-evoked norepinepherine release. *J Neurosci* **18:**8571–8579.

Margiotta J and Pugh P (2003) Nicotinic acetylcholine receptors in the nervous system, in *Molecular Insights into Ion Channel Biology in Health and Disease* (Maue RA ed), Elsevier, Amsterdam, in press.

Margiotta JF and Gurantz D (1989) Changes in the number, function and regulation of nicotinic acetylcholine receptors during neuronal development. *Dev Biol* **135:** 326–399.

McNerney M, Pardi D, Pugh P, Nai Q, and Margiotta J (2000) Expression and channel properties of $\alpha$-bungarotoxin-sensitive acetylcholine receptors on chick ciliary and choroid neurons. *J Neurophysiol* **84:**1314–1329.

Meyer EM, Tay ET, Papke RL, Meyers C, Huang GL, and de Fiebre CM (1997) 3-[2,4-Dimethoxybenzylidene]anabaseine (DMXB) selectively activates rat alpha7 receptors and improves memory-related behaviors in a mecamylamine-sensitive manner. *Brain Res* **768:**49–56.

Monod J, Wyman J, and Changeux J-P (1965) On the nature of allosteric transitions: a plausible model. *J Mol Biol* **12:**88–118.

Palma E, Eusebi F, and Miledi R (1997) Co-expression of the neuronal $\alpha_7$ and L247T $\alpha_7$ mutant subunits yields hybrid nicotinic receptors with properties of both wild-type $\alpha_7$ and $\alpha_7$ mutant homomeric receptors. *Proc Natl Acad Sci USA* **94:** 1539–1543.

Papke RL, Meyer E, Nutter T, and Uteshev VV (2000) $\alpha$7 Receptor-selective agonists and modes of $\alpha$7 receptor activation. *Eur J Pharmacol* **393:**179–195.

Pardi D and Margiotta JF (1999) Pituitary adenylate cyclase-activating polypeptide activates a phospholipase C-dependent signal pathway in chick ciliary ganglion neurons that selectively inhibits $\alpha$7-containing nicotinic receptors. *J Neurosci* **19:**6327–6337.

Penn AA, Riquelme PA, Feller MB, and Shatz CJ (1998) Competition in retinogeniculate patterning driven by spontaneous activity. *Science (Wash DC)* **279:** 2108–2112.

Pugh PC, Corriveau RA, Conroy WG, and Berg DK (1995) Novel subpopulation of neuronal acetylcholine receptors among those binding $\alpha$-bungarotoxin. *Mol Pharmacol* **47:**717–725.

Quik MW, Ceballos RM, Kasten M, McIntosh JM, and Lester RAJ (1999) $\alpha3\beta4$ subunit-containing nicotinic receptors dominate function in rat medial habenula neurons. *Neuropharmacology* **38:**769–783.

Ragozzino D, Fucile S, Giovanelli A, Grassi F, Mileo AM, Ballivet M, Alema S, and Eusebi F (1997) Functional properties of neuronal nicotinic acetylcholine receptor channels expressed in transfected human cells. *Eur J Neurosci* **9:**480–488.

Rakhilin S, Drisdel RC, Sagher D, McGehee DS, Vallejo Y, and Green WN (1999) $\alpha$-bungarotoxin receptors contain $\alpha$7 subunits in two different disulfide bonded conformations. *J Cell Biol* **146:**203–217.

Rezvani AH and Levin ED (2001) Cognitive effects of nicotine. *Biol Psychiatry* **49:**258–267.

Role LW and Berg DK (1996) Nicotinic receptors in the development and modulation of CNS synapses. *Neuron* **16:**1077–1085.

Ruiz M and Karpen JW (1999) Opening mechanism of a cyclic nucleotide-gated channel based on analysis of single channels locked in each conductance state. *J Gen Physiol* **113:**873–895.

Sargent PB (1993) The diversity of neuronal nicotinic acetylcholine receptors. *Annu Rev Neurosci* **16:**403–443.

Sivilotti LG, McNeil DK, Lewis TM, Nassar MA, Schoepfer R, and Colquhoun D (1997) Recombinant nicotinic receptors, expressed in *Xenopus* oocytes, do not resemble native rat sympathetic ganglion receptors in single-channel behaviour. *J Physiol* **500:**123–138.

Ullian EM, McIntosh JM, and Sargent PB (1997) Rapid synaptic transmission in the avian ciliary ganglion is mediated by two distinct classes of nicotinic receptors. *J Neurosci* **17:**7210–7219.

Vernallis AB, Conroy WG, and Berg DK (1993) Neurons assemble AChRs with as many as 3 kinds of subunits while maintaining subunit segregation among subtypes. *Neuron* **10:**451–464.

Weiland S, Bertrand D, and Leonard S (2000) Neuronal nicotinic acetylcholine receptors: from the gene to the disease. *Behav Brain Res* **113:**43–56.

Zhang Z-W, Vijayaraghavan S, and Berg DK (1994) Neuronal acetylcholine receptors that bind $\alpha$-bungarotoxin with high affinity function as ligand-gated ion channels. *Neuron* **12:**167–177.

**Address correspondence to:** Joseph F. Margiotta, Ph.D., Medical College of Ohio, Department of Anatomy and Neurobiology, Block Health Sciences Building, Room 108, 3035 Arlington Avenue, Toledo, OH 43614-5804. E-mail: jmargiotta@mco.edu.